

JOULE-THOMSON COEFFICIENTS OF
PROPANE AND N-BUTANE

Thesis by
Ronald Lee Smith

In Partial Fulfillment of the Requirements
For the Degree of
Doctor of Philosophy

California Institute of Technology
Pasadena, California

1970

(Submitted May 7, 1970)

ACKNOWLEDGMENTS

I wish to express my sincere appreciation to Professor B. H. Sage, my research advisor, for the guidance, interest and encouragement which he provided to me throughout the course of this study. Special thanks go to Professor W. H. Corcoran who assisted me during the later stages of this study. Thanks are also due to many other faculty members at the California Institute of Technology, especially those of the Department of Chemical Engineering. The contributions of my classmates are also acknowledged.

I am greatly indebted to the several sources of financial support which I received during the course of my graduate study: to the Standard Oil of California and to the California Institute of Technology for teaching and research assistantships.

Finally, I am grateful to my wife, Judy, for her patience and understanding during the time of research for and preparation of this thesis.

ABSTRACT

Experimental Joule-Thomson measurements were made on gaseous propane at temperatures from 100 to 280°F and at pressures from 8 to 66 psia. Joule-Thomson measurements were also made on gaseous n-butane at temperatures from 100 to 280°F and at pressures from 8 to 42 psia. For propane, the values of these measurements ranged from 0.07986°F/psi at 280°F and 8.01 psia to 0.19685°F/psi at 100°F and 66.15 psia. For n-butane, the values ranged from 0.11031°F/psi at 280°F and 9.36 psia to 0.30141°F/psi at 100°F and 41.02 psia. The experimental values have a maximum error of 1.5 percent.

For n-butane, the measurements of this study did not agree with previous Joule-Thomson measurements made in the Laboratory in 1935. The application of a thermal-transfer correction to the previous experimental measurements would cause the two sets of data to agree. Calculated values of the Joule-Thomson coefficient from other types of p-v-t data did agree with the present measurements for n-butane.

The apparatus used to measure the experimental Joule-Thomson coefficients had a radial-flow porous thimble and was operated at pressure changes between 2.3 and 8.6 psi. The major difference between this and other Joule-Thomson apparatus was its larger weight rates of flow (up to 6 pounds per hour) at atmospheric pressure. The flow rate was shown to have an appreciable effect on non-isenthalpic Joule-Thomson measurements.

Photographic materials on pages 79-81 are essential and will not reproduce clearly on Xerox copies. Photographic copies should be ordered.

TABLE OF CONTENTS

Acknowledgments	<u>Page</u>
	ii
Abstract	iii
List of Tables	v
List of Figures	vi

<u>Part</u>	<u>Title</u>	
I	Introduction	1
II	Literature	4
III	Experimental Apparatus	6
IV	Experimental Procedure	17
V	Thermodynamic Analysis	21
VI	Calculations	32
VII	Error Analysis	36
VIII	Results	39
IX	Conclusions	47
X	Future Work	49
XI	References	50
XII	Notation	55
XIII	Tables	58
XIV	Figures	77
XV	Appendices	91
XVI	Propositions	101

LIST OF TABLES

<u>Table</u>	<u>Description</u>	<u>Page</u>
1	Experimental Joule-Thomson Values for Propane	58
2	Corrected Joule-Thomson Values for Propane by Least-Squares Fit	60
3	Experimental Joule-Thomson Values for n-Butane	62
4	Corrected Differential Joule-Thomson Values for n-Butane by Least-Squares Fit	64
5	Equations for Isotherms	67
6	Calculated Values of the Joule-Thomson Coefficient at Zero Pressure from the Equation of Francis and Luckhurst	68
7	Calculated values of the Joule-Thomson Coefficient from the Benedict-Webb-Rubin Equation	69
8	Laboratory Instruments	70
9	Results of Thermocouple Calibration	71
10	Platinum-Resistance Thermometer Calibration	73
11	Results of Chromatographic Analysis	75
12	Comparison of Joule-Thomson Values of Previous Study Corrected for Thermal Transfer with Values of this Study for n-Butane	76

LIST OF FIGURES

<u>Number</u>	<u>Description</u>	<u>Page</u>
1	Schematic Diagram of Apparatus	77
2	Full-Scale Drawing of Calorimeter	78
3	Photograph of Calorimeter	79
4	Photograph of Calorimeter	80
5	Photograph of Calorimeter	81
6	Dimensionless-Temperature Profile of Porous Thimble Mounting Disc	82
7	Joule-Thomson Coefficients versus Pressure at Constant Temperatures: Propane	83
8	Joule-Thomson Coefficients versus Temperature at Constant Pressures: Propane	84
9	Joule-Thomson Coefficients of n-Butane versus Pressure at Constant Temperatures	85
10	Joule-Thomson Coefficients of n-Butane versus Temperature at Constant Pressures	86
11	Comparison of Experimental Joule-Thomson Coef- ficients for Propane with Equation of Francis and Luckhurst at Zero Pressure	87
12	Comparison of Experimental Joule-Thomson Coef- ficients for n-Butane with Equation of Francis and Luckhurst at Zero Pressure	88
13	Measurement of Joule-Thomson Coefficient During Approach to Steady-State	89
14	Comparison of the Joule-Thomson Values of the Previous Study Corrected for Thermal Transfer with those of this Study for n-Butane	90

I. INTRODUCTION

In the past ten years considerable interest, stimulated by the availability of high-speed computers, has arisen in relating macroscopic thermodynamic data to fundamental molecular properties [1].

Increasing knowledge of these relationships has generated the need for accurate and extensive thermodynamic measurements.

The Joule-Thomson coefficient is a thermodynamic quantity which can be used to increase the understanding of intermolecular forces [2,3,4,5]. It is defined as the differential change in temperature of a fluid with pressure at constant enthalpy and composition and is mathematically expressed:

$$\mu = \left(\frac{\partial T}{\partial P}\right)_{H, x_i} \quad (1)$$

By partial differentiation of the enthalpy when considered as a function of temperature and pressure, the Joule-Thomson coefficient can be expressed:

$$\mu = C_p^{-1} [T(\partial V/\partial T)_P - V] \quad (2)$$

where C_p is the heat capacity at constant pressure.

Several advantages of the Joule-Thomson coefficient are apparent from the above equations. Equation (1) indicates that only measurements of temperature and pressure are required to determine the Joule-Thomson coefficient for a constant enthalpy process. Since temperature and pressure can be measured with greater accuracy than volume, the Joule-Thomson coefficient offers a source of data of high accuracy. It

is the most useful thermodynamic quantity which requires no measurements of derived extensive properties in its determination.

From Equation (2) it can be shown that the Joule-Thomson coefficient is zero at all temperatures and pressures for an ideal gas. Therefore this coefficient is a direct measure of the non-ideal behavior of real fluids. When equations of state for real fluids, such as the virial equation [6], are inserted into Equation (2), the empirical constants which they contain can be determined from Joule-Thomson data [7,8]. If these constants have been previously related to microscopic properties, then the Joule-Thomson coefficient is related to the microscopic properties.

Although the Joule-Thomson coefficient can relate macroscopic measurements to microscopic properties, only fluids with the simplest molecular structures give consistent results. The lack of experimental measurements, especially at low pressures, has contributed to this inconsistency. More experimental measurements are needed on substances with complex molecular structures, especially the hydrocarbons and their mixtures. In the paraffin series where molecular similarity is evident and the cost of high-purity materials is not prohibitive, the amount of data is limited. A recent collective reference [9] indicated most measurements of the paraffin hydrocarbons were made prior to 1940 and included no molecular weights higher than pentane. Some regions of temperature and pressure are totally excluded and the duplication of experimental measurements is almost non-existent. No measurements of the Joule-Thomson coefficient for any substance were found below atmospheric pressure.

The sparseness of data is emphasized by the lack of correlation between present theory and experimental measurements. Manning and Canjar [10] showed that Joule-Thomson coefficients calculated from equations of state such as the virial and Benedict-Webb-Rubin [11] equations deviate from experimental measurements by an unexplainable amount. Francis and Luckhurst [12] showed the data on normal paraffin hydrocarbons with molecular weight higher than ethane do not conform to their equation relating to the corresponding states theory within experimental and theoretical uncertainties. Present theories or experimental Joule-Thomson values must be improved for molecules with complicated structures. More experimental measurements are required for either alternative.

This particular research program was undertaken to build an apparatus for measuring the Joule-Thomson coefficients of the paraffin hydrocarbons. Measurements were taken on propane and n-butane at pressures below 75 psia. Many measurements were made below atmospheric pressure. This region is of important theoretical interest.

II. LITERATURE

The classic experiments of Joule and Thomson [13,14] concerning the temperature change resulting from the free expansion of gases were performed between the years 1852 and 1862. Since their classic experiments, progress has been slow and irregular. The decades prior to 1920 produced data which were generally limited in scope and lacking in experimental precision [15,16,17]. Measurements were made on only the most common gases such as water vapor, nitrogen, carbon dioxide and air. One significant contribution of this period, even though neglected until the 1920's, was the change in the method of throttling from orifices, valves and axial flow porous materials to radial flow porous thimbles [15,16].

During the next twenty years, emphasis was placed on experimental measurements of the Joule-Thomson effect and on empirical equations of state to express the data. Two very active experimental groups during this period were Roebuck and co-workers [19 through 27] at the University of Wisconsin on inorganic gases, and Sage and co-workers at the California Institute of Technology on hydrocarbons. This latter group obtained data [28 through 35] on methane, ethane, propane, n-butane, n-pentane and mixtures of methane-ethane, methane-n-butane and methane-propane.

Just prior to the 1940's interest began to wane because of World War II. A publication by Hirschfelder and co-workers [2] in 1938 set the stage for later renewed interest. This paper pointed out that Joule-Thomson coefficients can make a significant contribution to the understanding of intermolecular forces.

The development of the computer, in conjunction with statistical mechanics and the more complicated equations of state, has made this relationship between intermolecular forces and Joule-Thomson coefficients more important [3,4,5]. As indicated in a brief summary of recent Joule-Thomson studies by Potter [1], present-day interests are along the lines of improved Joule-Thomson measurements through improved equipment and techniques, more extensive measurements including mixtures, and better correlation of experimental data with fundamental molecular properties. Up to now, only gases with the simplest molecular structures and correspondingly small Joule-Thomson effects give good agreement between experiment and theory. In general, the higher molecular weight materials with more complicated force structures give poor agreement, either due to the model used or accuracy of the experimental data.

III. EXPERIMENTAL APPARATUS

A schematic diagram of the Joule-Thomson apparatus employed in this study is presented in Figure 1. The description of this apparatus is divided into two parts: (A) the calorimeter, and (B) the auxiliary equipment. The Joule-Thomson expansion took place in the calorimeter. The auxiliary equipment consists of all other components of the system used to maintain and control the flow of gas to and from the calorimeter. Final design of the calorimeter and auxiliary equipment was based on laboratory experiments and their analysis, along with previous Joule-Thomson apparatus [28,31,36] used in the Laboratory. Laboratory tests during the early stages of this study indicated measurement of the temperature change to be a major problem. All construction of the experimental apparatus was done by the author.

A. CALORIMETER

A scale drawing of the calorimeter used for the measurements on propane and n-butane is given in Figure 2. Photographs at various stages of assembly are presented in Figures 3 through 5. Figure 3 illustrates the individual components from which the calorimeter was constructed. The mounting disc for the porous thimble is in the center of this photograph. The small tubes protruding upward from the disc are thermocouple wells. Just to the left of the mounting disc is the porous thimble. Attached to the base of the thimble is its mounting flange. The eight cylinder-shaped objects in the picture are radiation heat shields. The inner and outer radiation-shield mounting rings lie at the left and right ends of the ruler.

All parts of the calorimeter were easily assembled and disassembled. Stainless-steel screws were used to hold the thimble and mounting rings in place. The ease of assembly and disassembly permitted the measurement of Joule-Thomson coefficients with different arrangements of the radiation shields. Nitrogen and carbon dioxide were used as test gases. These gases could be exhausted to the atmosphere. At room temperature and atmospheric pressure, the values of their Joule-Thomson coefficients were sufficiently different that they spanned the anticipated range of the hydrocarbon measurements.

The mounting disc for the porous thimble was machined from a linen-base, phenolic plastic. This plastic has excellent high-temperature and chemical-resistance properties. It is easy to machine and is also a good thermal insulator. The diameter and thickness of the disc were limited by the size of the cavity in the pressure vessel designed for measurements from 50 to 5000 psia. Since all unwanted heat transfer occurred through this disc, it was made as thick as practicable. A Teflon mounting disc was also tested but the difficulty in attaching thermocouple wells and exhaust tubing eliminated it from consideration. After the gas passed through the thimble, it exited from the calorimeter through the 0.814-inch hole in the center of the mounting disc.

Twelve 0.020-inch stainless-steel tubes protrude from the mounting disc. They served as thermocouple wells for two separate thermocouple networks. Three tubes with an angular spacing of 120° were mounted at each of the four radial distances indicated for thermocouples in Figure 2. With the calorimeter assembled, each thermocouple network

had three tubes inside the thimble and three outside. The external thermocouple network consisted of three tubes at both the largest and smallest radial distance. The internal network was composed of the remaining tubes. The external network was displaced by 60° angular rotation to the internal network.

Thermocouples were easily removed from the thermocouple wells without damage. The networks were also interchangeable. This feature eliminated early doubts as to whether different thermocouple readings were due to differences in the networks or to temperature gradients inside the thimble. The different lengths of the thermocouple wells were due, in part, to the different heights of the radiation shields which enclosed them. Measurement of the temperature change was made as far away from the thimble mounting disc as practical. This reduced the effects of any thermal gradients in the mounting disc. The thermocouple tubes were small in diameter to insure rapid response. In early prototypes the thermocouple wells were open and the thermocouples were epoxied in place. An erratic temperature in an early test was blamed on gas leaking past the epoxy and jetting on the thermocouple junction. Closed thermocouple wells prevented this problem with only a minor loss in response time. The use of three thermocouples in series for each thermocouple network was based on prior experiences in the Laboratory and no other combination was tested.

Both thermocouple networks had copper-constantan junctions. All thermocouple wire was 0.005-inch diameter and Teflon coated. Selection of copper-constantan junctions was based on the greatest response to temperature changes. Both thermocouple networks measured the

temperature of the gas after passing through the thimble relative to the gas temperature before expansion. Therefore the measured temperature change was almost independent of the inlet or exit gas temperature measurements.

The porous thimble used in this project was obtained from Coors' Porcelain Company in Golden, Colorado. It was made from a fine-grained alundum material. This thimble was machined on both its inside and outside surfaces after receipt from Coors. Permeability tests on the uncut thimble indicated that a wall thickness of 0.040 inch would give a flow rate of 125 standard cubic feet of nitrogen per hour with a pressure change from two to one atmospheres absolute. Machining of the wall surfaces also improved the uniformity of the porous thimble, thereby reducing the mixing problem. A small rim was left at the base of the thimble for the flange mounting ring. The end of the thimble was machined flat and then polished for a better seal at the thimble mounting disc. A groove in the mounting disc centered the thimble and confined the Teflon gasket used for the mounting seal.

Four thimbles, three alundum and one gold-platinum, were tested in one or more of the four test calorimeters during the design stage. All of the thimbles remained from the Joule-Thomson study on steam [36]. The shape of the porous surface was not tested as all of the thimbles had the same basic shape. One attempt to test a spherical porous surface ended in failure due to mechanical problems. A spherical porous surface with a high ratio of porous surface to mounting surface is theoretically a better design.

Tests with the alundum thimbles consisted of changing the wall thickness and reducing the flow area by using an impervious coating. The gold-platinum thimble was tested in three different conditions: as received with its eighteen 0.006-inch diameter holes partially clogged, all eighteen holes opened, and all eighteen holes increased to 0.008-inch diameter. Test results with the gold-platinum thimble were similar to the alundum thimbles except for larger fluctuations in the measured temperature change. The larger fluctuations were contributed to the mixing of the expanded gas. Two thermocouple networks, similar to those previously described, measured the results of all tests.

At low flow rates both thermocouple networks indicated temperature changes smaller than anticipated. Agreement of nitrogen and carbon dioxide with published values [9] improved with increasing flow rates. An explanation of this result is explained later (see Thermodynamics Analysis). In addition, the two thermocouple networks did not give identical results when the calculated Reynolds number in the annular region between radiation shields was in the laminar region (below 2000). The Reynolds number at a particular weight rate of flow of the gas was changed by increasing or decreasing the number of radiation shields. At low Reynolds numbers, the interior thermocouple network indicated a smaller temperature change than the external network. If this difference had been caused by thermal transfer, the external network would have indicated the smaller change. The difference in values was credited to poor mixing of the expanded gas. At flow rates with Reynolds numbers above 2500, the difference was negligible and the gas was assumed to be mixed.

The eight radiation-heat shields used in the calorimeter were made of 0.001-inch brass shim stock. Five of the shields were nested concentrically around the thimble. The other three were located concentrically within the thimble. The cylindrical shape of each radiation shield was maintained by a small brass ring at one end of the shield and the plastic mounting ring at the other end. The brass ring had cross-sectional dimensions of 0.050 by 0.050-inch. All seams were soldered. A two-mil gold plating, both inside and out, was used to prevent corrosion in future anticipated measurements. Primary purpose of the radiation shields was to increase the turbulence of the gas and to direct the flow past the thermocouples. The final design and arrangement of the radiation shields were determined by several factors. Length of the radiation shields was limited by the dimensions of the thimble and by the cavity of the high-pressure vessel. The number of shields used was a compromise. Increasing the number of shields between the thimble and thermocouples reduced the fluctuations in thermocouple readings. Decreasing the number of shields reduced the kinetic energy change. Two shields between the thimble and thermocouples on each side of the thimble was the best arrangement tested.

Each radiation shield was individually removable and electrically insulated from the other shields. Removable shields made possible a larger number of tests. Electrically insulated shields reduced the possibility of thermocouple shorts. The shields were attached to the mounting rings by a press-fit and then pinned to prevent any slippage that might occur at the higher temperatures of the investigation. The gas flowed between shields in an axial direction

because the holes alternated between the top and base of adjacent radiation shields. These holes are easily seen in Figure 3. One exception to the axial flow between adjacent shields was the two outermost shields where no flow occurred to increase thermal resistance. The annular cross-sectional area between adjacent shields exterior to the thimble was 0.745 in^2 . Interior to the thimble, the area was 0.521 in^2 . Ideally, the larger cross-sectional area should have been interior to the thimble, but a minimum clearance of 0.090-inch between adjacent shields exterior to the thimble made the ideal case impractical.

The calorimeter was housed in a pressure vessel. Two pressure vessels were constructed for this study; one for pressures below 75 psia and a second for pressures from 50 to 5000 psia. The low-pressure vessel was made from a fourteen-inch section of 9.5-inch diameter brass pipe with a wall thickness of 1/4-inch. The top and bottom of the vessel were made from 1/4-inch brass plate, reinforced by 1/2-inch steel plates which also served as flanges for securing the top and bottom. Teflon gaskets were used for seals between the top and bottom with the sides. Since the high-pressure vessel was not used in this study, it will not be described even though its construction was completed.

An exhaust line, which connected to the rear of the mounting disc, served as the mounting for the calorimeter. This exhaust line, which was thermally insulated, made a 90° turn inside the pressure vessel and exited through the sides of the vessel. A flange in this line permitted the removal of the calorimeter. Passage of the exhaust

line through the sides of the vessel allowed the top of the vessel to be removed without disturbing the calorimeter.

Pressure measurements of the gas prior to throttling were taken from a pressure tap on the side of the pressure vessel. A second pressure tap was located on the exhaust line at the rear of the mounting disc. Since the exhaust line had an inside diameter of 1 inch, no pressure correction was made for the distance between the thermocouples inside the thimble and the exhaust-pressure tap. A mercury manometer, connected to the two pressure taps, measured the pressure change across the thimble. Pressure at the second tap was calculated from the absolute pressure at the first tap and the change in pressure between taps.

The temperature of the gas prior to throttling was measured by a platinum thermometer. This thermometer was located in the oil bath adjacent to the pressure vessel. Prior tests on carbon dioxide with a differential thermocouple indicated no detectable temperature difference between the oil bath and gas inside the pressure vessel. Calibrations of the temperature and pressure-measuring instruments are covered in Appendices I and II, respectively.

Up to now, only the positive side of the design changes has been discussed. Compromises were sometimes made. A comparison of the new Joule-Thomson calorimeter with the calorimeter used for measuring the Joule-Thomson coefficients of steam was made. Merits of both the old and new were included.

The change which laboratory tests indicated most significant was the increased flow rate of the new calorimeter. This change was

incorporated by reducing the wall thickness of the porous thimble from 0.125-inch to 0.040-inch and by operating the equipment at pressure changes up to 8.6 psi. The increased flow rate through the calorimeter made other changes necessary. These changes were primarily the result of the increased volumetric flow rate, especially at low pressures. The increased flow rate decreased the thermal-transfer correction (see Thermodynamics Analysis), response time, and mixing problems. On the other hand, problems with kinetic energy changes, equipment size and auxiliary-flow equipment resulted from the increased flow rate. To reduce the kinetic energy change, a pressure vessel with large passages and restricted for use at low pressures was necessary. This caused the construction of a second pressure vessel with smaller passages to reduce structural stresses at high pressures. The changing of equipment in the middle of an investigation is not desirable.

Another change was the use of 0.001-inch brass radiation shields in place of the 0.010-inch brass or 0.020-inch gold shields of the steam calorimeter. The increased flow rates of the gas and smaller mass of the radiation shields reduced the time to attain steady state from days to hours. The smaller mass did not dampen temperature fluctuations as well and this placed more stringent requirements on pressure regulation. The use of equal annular areas between adjacent radiation shields rather than equal radial distances improved the accuracy of the kinetic energy calculations but complicated construction. The use of plastic instead of stainless-steel for the mounting disc reduced thermal transfer and also the maximum operating temperature of the calorimeter.

B. AUXILIARY EQUIPMENT

The components of the Joule-Thomson apparatus making up the auxiliary equipment are shown in Figure 1. The auxiliary equipment is described in the same order that the experimental fluid followed as it flowed through the different components. The hydrocarbon gas was stored as a liquid in one of the two high-pressure storage cylinders. Each cylinder held about 20 pounds of liquid hydrocarbon. The equipment was arranged so that either cylinder could be removed or replaced during an experiment without affecting the measurements. Each cylinder was wrapped with an 800-watt tape heater. These heaters were used to increase the vapor pressure of the liquid hydrocarbon. Vapor pressure was the source of pressure for all experimental measurements. Pressure gauges on each storage cylinder recorded the vapor pressure. The output of the heaters was controlled manually by Variacs.

A 1/4-inch copper tube connected the hydrocarbon cylinder manifold to a vaporizer. The vaporizer consisted of about thirty feet of 1/4-inch copper tubing coiled around a twelve-inch length of 2-inch o.d. brass pipe. Inside the pipe were about fifty feet of nichrome heating wire coiled on a ceramic tube. The vaporizer was installed with the pipe in a vertical position. A 1/4-inch copper tube connected the vaporizer to a pressure regulator which was located about eighteen inches above it. Additional 1/4-inch tubing connected the regulator to a valve panel. This panel consisted of five valves and two rotameters. The arrangement of this panel can be seen in Figure 1. The rotameters were to determine the composition of gas mixtures.

The next component in the flow path was a Cartesian manostat which regulated the pressure to the nearest 0.1 mm Hg. After passing the manostat, the gas entered a second electrical heater similar to the vaporizer and designated as a preconditioning heater. The gas then flowed through fifty feet of 1/4-inch copper tubing which was submerged in the oil bath. After passing through the conditioning tubing, the gas flowed into the pressure vessel which was also located in the oil bath. The gas then flowed through the calorimeter and passed from the pressure vessel through the exhaust line.

The oil bath and thyatron temperature modulator were of the standard design used in the Laboratory.

After passing from the pressure vessel by a 1-1/4-inch o.d. heavy-wall brass pipe, the gas flowed through a large throttle valve. After the throttle valve, it flowed into one of two high-pressure cylinders which were submerged in a dry ice - trichloroethylene mixture. It was possible to remove and replace the receiving cylinders during a measurement without disturbing the steady state. A vacuum pump could be connected to the receiving cylinder manifold.

IV. EXPERIMENTAL PROCEDURE

The equipment used for the Joule-Thomson measurements has been previously described (see Experimental Apparatus). Measurements began by setting the controls on the constant-temperature oil bath, which contained the Joule-Thomson calorimeter, for the desired temperature. Usually four to eight hours elapsed until the interior of the calorimeter came to thermal equilibrium with the oil bath. This elapsed time could be reduced by a small flow of gas through the calorimeter. A zero temperature change across the porous thimble was used as an indication of equilibrium. The liquid hydrocarbon was warmed by the heaters on the high-pressure storage cylinders as the bath and calorimeter were brought to temperature. Due to various line, valve, and regulator pressure losses, the vapor pressure for any measurement was normally 25 to 50 psi higher than the pressure at the inlet of the calorimeter.

The hydrocarbon cylinders were inverted so that liquid rather than vapor left the cylinder. This was necessary because the heat of vaporization at the liquid-gas interface was large. In tests with carbon dioxide where the liquid-gas interface was inside the cylinder, large quantities of heat were required to maintain a constant cylinder temperature. Temperature regulation was very difficult due to the delay in response to changes in heater settings. Maintaining a constant temperature and vapor pressure inside the heavy-walled cylinder improved pressure regulation.

When liquid was removed from the cylinder, the liquid-gas interface was outside the storage cylinder. The vaporizer with its more efficient heat exchanger and faster response vaporized the liquid and superheated the vapor. This latter feature was particularly desirable. It prevented condensation of the gas cooled by the Joule-Thomson expansion upon passing through the pressure regulator. During start-up the superheat helped to heat the copper tubing between the vaporizer and pressure regulator. The vertical position of the vaporizer allowed any condensation to drain back to the liquid-gas interface. The poor thermal conductivity of gases relative to liquids aided temperature regulation at the vaporizer.

After passing from the vaporizer, the superheated gas entered the pressure regulator used to maintain a pressure of about 10 psi higher than that desired for the particular measurement. This extra 10 psi was removed by throttling the gas at the valve panel. Throttling was necessary for the proper operation of the Cartesian manostat located after the valve panel in the direction of flow. The manostat controlled the pressure to 0.1 mm Hg by bleeding off the excess. The throttle valve reduced the volume of gas lost at the manostat. The amount was determined by bubbling through a beaker of water. The optimum volume was the lowest that constantly bubbled through the water. It amounted to a few cubic centimeters of gas per hour.

After passing the manostat, the gas entered the preconditioning heater which adjusted the gas temperature to that of the oil bath. A

mercury thermometer was used to determine the initial heater settings. Final adjustments were determined by the automatic feature of the thyatron temperature controller on the oil bath. If the gas temperature was too low after leaving the preconditioning heater and upon entering the conditioning coil submerged in the oil bath, the bath required more power to maintain a constant temperature than it did just prior to the start of the gas flow. When the gas departed the preconditioning heater at the proper temperature, the automatic controller returned to its original setting. The conditioning coil in the oil bath made the final temperature adjustment to the gas before entering the calorimeter pressure vessel also submerged in the oil bath.

After entering the pressure vessel, the gas flowed into the calorimeter and through the porous thimble. The pressure change and the temperature change of the throttling process were measured in the calorimeter. The exhaust pressure of the calorimeter was regulated by a large throttle valve located approximately six feet downstream from the calorimeter. When the throttle valve was completely closed there was no pressure change across the thimble. By slowly opening this valve, the desired pressure change across the thimble could be obtained. Remember that the upstream pressure was controlled by the regulator-manostat and essentially independent of the downstream pressure. During start-up this valve was always closed to prevent an excessive pressure change across the porous thimble.

After passing through the large throttle valve, the gas entered one of two high-pressure receiving cylinders. These cylinders were evacuated prior to each experiment and submerged in a dry ice -

trichloroethylene bath. The hydrocarbon gas recondensed and the vapor pressure reduced to a few centimeters of mercury. This low pressure extended back to the large throttle valve in the exhaust line from the calorimeter. The large pressure drop across this valve caused a sonic velocity through it which eliminated the effects of any pressure fluctuations in the receiving cylinders. Proof of this sonic velocity was determined by adjusting valves on the receiving cylinder manifold without disturbing the Joule-Thomson measurement. The condensation process also acted as a leak detector for the measurements below atmospheric pressure. Had any non-condensables leaked into the apparatus, it would have would have increased the pressure inside the receiving cylinders.

Since both the storage and receiving cylinders could be replaced during an experiment, the initial amount of liquid in the storage cylinders was not a limiting factor. No run used more than 40 pounds of hydrocarbon.

V. THERMODYNAMIC ANALYSIS

The Joule-Thomson coefficient of a fluid is defined as its differential change in temperature with pressure at constant enthalpy and composition. All apparatus for measuring Joule-Thomson coefficients as functions of temperature and pressure are basically similar. A fluid maintained at a constant temperature and pressure is throttled under steady-flow conditions into a region of lower pressure. Only measurements of temperature and pressure are required with the ideal conditions of constant enthalpy and composition. However, a Joule-Thomson expansion at constant enthalpy is most difficult due to thermal transfer and kinetic energy changes within the experimental system.

Mathematical relationships to analyze the effects of non-constant enthalpy on the Joule-Thomson coefficients are derived from thermodynamics. Unlike the ideal case, the equations emphasize the effects of the flow rate through the porous thimble on experimental measurements. The model represents the limiting case for thermal transfer and was used to evaluate the design and operation of the Joule-Thomson apparatus. It was also used to analyze two methods of measuring Joule-Thomson coefficients and to correct previous Joule-Thomson measurement for thermal transfer (see Results).

To develop the mathematical relationships, an extension of the Gibbs phase rule [27] was used as the starting point. The state of a homogeneous fluid of constant composition is a unique function of two intensive variables. The temperature was considered a function of pressure and enthalpy:

$$T = f(P,H) \quad .$$

The total derivative of the temperature with respect to pressure is

$$(dT/dP)_{\text{path}} = (\partial T/\partial P)_H + (\partial T/\partial H)_P (dH/dP)_{\text{path}} \quad (1)$$

The "path" is the course which the fluid takes as it flows between the temperature and pressure-measuring devices in the throttling calorimeter. Notice that the measured change in temperature with pressure is path dependent, even though the Joule-Thomson coefficient, $(\partial T/\partial P)_H$, is independent of the path. For small changes in pressure, Equation (1) can be expressed as

$$(\Delta T/\Delta P)_{\text{path}} = (\partial T/\partial P)_H + (1/C_p) (\Delta H/\Delta P)_{\text{path}} \quad (2)$$

where C_p is defined as $(\partial H/\partial T)_P$.

The law of conservation of energy for a steady flow process was used to evaluate ΔH . This law can be expressed

$$Q' - W'_s = \Delta H + \Delta(P.E.) + \Delta(K.E.)$$

where Q' and W'_s represent the thermal transfer and shaft work per pound of fluid. If the potential energy change is small and no shaft work is performed, the above equation reduces to

$$Q' = \Delta H + \Delta(K.E.) \quad (3)$$

Solving for ΔH in Equation (3) and substituting the results into Equation (2)

$$(\Delta T/\Delta P)_{\text{path}} = (\partial T/\partial P)_H + (1/C_p) \{ [Q' - \Delta(K.E.)] / \Delta P \}_{\text{path}} \quad (4)$$

To calculate a value for the thermal transfer, Q' , it is necessary to understand the mechanics of the throttling process. Thermal transfer results from the temperature change of the expansion. Heat is either added to or lost from the throttled fluid, according to whether the fluid is cooled or heated upon expansion. Since the expanded fluid is in contact with both the interior surface of the porous thimble and the surface of the mounting disc enclosed by the porous thimble, heat can be transferred through either surface. For simplicity in calculation, thermal transfer through the walls of the thimble and through the mounting disc were handled separately by alternately assuming the other to be a perfect thermal insulator.

In the first case, the mounting disc for the porous thimble was assumed a perfect thermal insulator, while the fluid and porous thimble were treated as thermal conductors. The fluid, prior to passing through the porous thimble, had a temperature and pressure of T_1 and P_1 . The temperature and pressure of the fluid after passing through the thimble were T_2 and P_2 . The fluid was assumed to have a positive Joule-Thomson coefficient. Therefore T_2 and P_2 are lower in value than T_1 and P_1 . Since the walls of the thimble and fluid have finite thermal conductivities, a heat flux in the direction of the fluid flow occurred across the thimble due to the temperature change. No heat was lost by conduction through the mounting disc since it was assumed a perfect thermal insulator. Therefore the source of the heat transmitted by thermal conduction through the walls of the thimble was from the fluid prior to passing through the thimble. The

fluid which released this heat was then cooler than T_1 prior to being throttled. However, all heat conducted through the walls of the thimble must be returned to the expanded gas since no heat accumulated in the walls and no heat was conducted through the mounting disc. The expansion is isenthalpic and therefore the state of the throttled fluid was uniquely determined by P_2 and H_2 . The net result was no change to the Joule-Thomson measurements because of thermal transfer through the walls of the thimble. Therefore a gold thimble would give the same results as one of low thermal conductivity. A temperature gradient in the fluid adjacent to the thimble was possible. Turbulence of the fluid, aided by the radiation shields, reduced the effects of this gradient on the experimental measurements to a non-detectable amount.

Thermal transfer through the mounting disc for the porous thimble occurred because the expanded gas inside the thimble was cooler than the inlet gas which was in contact with the external surfaces of the mounting disc. If the temperatures of all surface areas of the thimble mounting disc were known, it would be theoretically possible to calculate the thermal transfer through that part of the mounting disc surface enclosed by the porous thimble. The amount of thermal transfer would be calculated in BTU's per hour since no quantity used in the calculation is related to the flow rate. The temperature change which caused the thermal transfer is primarily a function of the pressure change and Joule-Thomson coefficient of the fluid and almost independent of the permeability of the porous thimble. Since "Q" in Equation (4) was given in BTU's per pound of fluid, it is related to the thermal transfer calculated from the surface temperatures of the mounting disc

in BTU's per hour through the flow rate. This relation can be expressed mathematically as

$$Q' = \dot{Q}/\dot{m} \quad (5)$$

where \dot{Q} is the thermal transfer in BTU's per hour and \dot{m} the flow rate in pounds per hour.

Substituting Equation (5) into Equation (4), the following relation was found:

$$(\Delta T/\Delta P)_{\text{path}} = (\partial T/\partial P)_H + (1/C_p) \{[(\dot{Q}/\dot{m}) - \Delta(\text{K.E.})] / \Delta P\} \quad (6)$$

It is evident at this point that experimental measurements of the Joule-Thomson coefficient are dependent on the flow rate due to non-isenthalpic conditions. Rearranging Equation (6), one obtains:

$$(\Delta T/\Delta P)_{\text{path}} = (\partial T/\partial P)_H + \dot{Q}/\dot{m} C_p \Delta P - \Delta(\text{K.E.}) / C_p \Delta P \quad (7)$$

To aid in subsequent analysis, the last two terms on the right-hand-side of Equation (7) will be designated by

$$C_{\dot{Q}} = \dot{Q}/\dot{m} C_p \Delta P \quad (8)$$

$$C_{\Delta(\text{K.E.})} = \Delta(\text{K.E.}) / C_p \Delta P \quad (9)$$

In the above equations, ΔP represents $P_2 - P_1$ and is negative. Therefore the thermal-energy correction subtracts from the true value of the Joule-Thomson coefficient and the kinetic energy correction adds to the true value.

Before using Equation (7) to calculate numerical values of the thermal and kinetic energy corrections for the apparatus used in this

study, the equation will be used to analyze two methods of measuring Joule-Thomson coefficients.

One successful method of measuring Joule-Thomson coefficients has been through the use of large pressure changes. These changes usually range from 300 to 1000 psi. Using large changes reduces the percent error caused by instrumentation inaccuracies. It does not reduce the thermal-transfer correction because the pressure change appears in the denominator. As ΔP is increased, ΔT increases somewhat proportionally. The amount of thermal transfer increases with the increase in ΔT . However, the flow rate through the thimble also increases and it is not offset by any term in the numerator of Equation (8). The increased flow rate reduces the error in Joule-Thomson coefficients measured with large pressure changes since the thermal-energy correction is normally neglected due to the difficulty in calculating values for the thermal transfer. Unfortunately the resulting Joule-Thomson coefficients are integral values, and the differential coefficients must be calculated. The calculations introduce errors to the differential coefficient, thereby reducing a part of the advantage of the method. A major disadvantage is that measurements near zero pressure are not possible.

A second successful method of measuring Joule-Thomson coefficients has been to use small pressure changes of less than one atmosphere. It is assumed that the differential Joule-Thomson coefficient is measured directly by this method. Small pressure changes are usually accompanied by small volumetric-flow rates. Small volumetric-flow rates result in even smaller weight-flow rates at low pressures. As

the weight-flow rate approaches zero, the correction due to thermal-energy transfer approaches infinity if the pressure change remains constant. This result can be determined from Equation (8). Therefore the method of small pressure changes is subject to large errors at low pressures.

This particular study used the method of small pressure changes but incorporated one feature of the large pressure change method. The porous thimble had very thin walls so large flow rates could be obtained at low pressures. Flow rates up to five pounds per hour were obtainable below atmospheric pressure. Several problems occurred as a result of the high flow rates. Large passages in the calorimeter were required to reduce kinetic energy changes. These large passages made necessary the construction of a second pressure vessel with small passages for high pressures. Pumping large volumes of low density gases caused many problems. This was solved by a single-pass evaporation-condensation pumping system. Other than mechanical problems, the method of small pressure changes combined with large flow rates has no major disadvantages. Its most important feature was its high accuracy in the low pressure region where the other methods are not possible or are subject to large inaccuracies.

As the correction factors for thermal transfer and kinetic energy changes are path dependent, the following numerical calculations apply only to the equipment used in this study. The principle is applicable to most Joule-Thomson apparatus. The first correction to be inspected will be that due to kinetic energy changes.

Kinetic energy changes were caused primarily by changes in the specific volume of the gas resulting from the pressure change. Since the slope of the specific volume versus pressure curve of a gas increases with decreasing pressure, the largest changes in volume occurred at the lowest pressure for a particular ΔP . This result can be seen from the ideal gas law:

$$d(V)/dP = d(RT/P) / dP = -RT/P^2 .$$

Some of the larger pressure changes in this study occurred at the lower pressures to increase the weight-flow rate through the thimble.

Three assumptions were used in the correction for the kinetic energy change: the ideal gas law is applicable, average velocities can be used, and the temperature change due to the throttling can be neglected. At low pressures and small temperature changes, all three assumptions are reasonable. The gas flowed in the annular space between the radiation shields before and after the Joule-Thomson expansion. The cross-sectional area between adjacent shields exterior to the thimble was 0.745 in^2 . Interior to the thimble it was 0.521 in^2 .

Changes in kinetic energy per pound of fluid can be expressed in terms of average velocities by

$$\Delta (\text{K.E.}) = (u_2^2 - u_1^2) / 2g_c \quad (10)$$

where u_1 and u_2 are the velocities of the gas before and after throttling, and g_c is the gravitational constant. Substituting Equation (10) into Equation (9), one obtains

$$C_{\Delta(\text{K.E.})} = (u_2^2 - u_1^2) / 2g_c C_p \Delta P \quad .$$

Incorporating geometrical factors of the calorimeter and using the ideal gas law, it results that

$$C_{\Delta(\text{K.E.})} = [(\dot{m}^2 R^2 T^2) / 2g_c C_p (P_2 - P_1)] [(1/P_2^2 A_2^2) - (1/P_1^2 A_1^2)] \quad . \quad (11)$$

The maximum kinetic energy correction occurred in a propane experiment where $P_1 = 12.30$ psia, $P_2 = 3.72$ psia, $T = 740^\circ\text{R}$ and $C_p = 0.522$ BTU/lb $^\circ\text{R}$. Using these values, the solution to Equation (11) is

$$C_{\Delta(\text{K.E.})} = - 5.89 \dot{m}^2 \times 10^{-5} \text{ }^\circ\text{R/psi} \quad .$$

Since the flow rates at the above conditions was 3.31 pounds per hour, the kinetic energy change correction was 6.4×10^{-4} $^\circ\text{R/psi}$ or about 0.8% of the measured coefficient. (Propane at 280°F and 8.01 psia has a Joule-Thomson coefficient of $0.07986^\circ\text{F/psi}$). At 15.38 psia and 280°F , the kinetic energy correction decreased to approximately 0.38% of the measured coefficient even though the flow rate was increased to 7 pounds per hour.

An exact calculation of the thermal transfer, \dot{Q} , is virtually impossible but an estimate of the upper limit was made. Four assumptions were necessary: (1) the throttled fluid was assumed to be in thermal equilibrium with the surface of the mounting disc enclosed by the porous thimble, (2) all other surfaces of the mounting disc were at the temperature of the inlet gas, (3) the expanded gas was perfectly mixed and (4) the cylindrical mounting disc could be approximated by a

bar of the same cross-sectional profile and equivalent heat-transfer areas on the top and bottom. Using these assumptions, the temperature profile of the mounting disc was determined numerically using a relaxation method described by Dusenberre [38]. A one-eighth inch square grid was used in the calculations. A solution was determined for a dimensionless temperature defined by

$$\phi = (T - T_1) / (T_2 - T_1) \quad .$$

The resulting temperature profile for a radial cross-section of the mounting disc is given in Figure 6. A value of $(\Delta\phi/\Delta y)_{y_0}$ was found to be -0.888/inch where y is the coordinate direction perpendicular to the lower surface of the mounting disc and y_0 represents the lower surface.

The thermal transfer into the interior of the thimble was calculated from the equation:

$$\dot{Q} = -kA_o (dT/dy)_{y_0} \approx kA_o \Delta T (\Delta\phi/\Delta y)_{y_0} \quad (12)$$

where $\Delta T = T_2 - T_1$. Substituting Equation (12) into Equation (8)

$$C_{\dot{Q}} = [kA_o (\Delta\phi/\Delta y)_{y_0}] (1/C_p) (1/\dot{m}) (\Delta T/\Delta P) \quad . \quad (13)$$

The term in the brackets is constant for any particular apparatus since it depends only on the materials of construction and shape of the heat transfer surface. It was calculated for the case where $A_o = 1.885 \text{ in}^2$, $k = 8.5 \times 10^{-3} \text{ BTU/hr-in-}^\circ\text{F}$, and $(\Delta\phi/\Delta y)_{y_0} = -0.888/\text{inch}$. The result of this calculation was

$$C_Q = -0.014(1/C_p)(1/\dot{m})(\Delta T/\Delta P) \text{ } ^\circ\text{F}/\text{psi}$$

The percent of the Joule-Thomson coefficients given by the thermal-energy correction is

$$C_Q / (\Delta T/\Delta P) = -0.014 (1/C_p)(1/\dot{m}) \times 100 \quad . \quad (14)$$

Equation (14) implies that a gas with a $C_p = 0.5 \text{ BTU}/\text{lb-}^\circ\text{F}$ and flowing through the thimble at a rate of 1 pound per hour would result in a Joule-Thomson coefficient that is too small by 2.8%. Between 100 and 280^oF, the constant pressure heat capacity of both propane and n-butane at zero pressure range between 0.4125 and 0.5225 BTU/lb-^oF, according to Rossini [39].

Returning to the same example used in the kinetic energy correction (propane at 280^oF and 8.01 psia with $C_p = 0.522 \text{ BTU}/\text{lb-}^\circ\text{F}$ and $\dot{m} = 3.31$ pounds per hour), the thermal energy correction is $-6.45 \times 10^{-4} \text{ } ^\circ\text{F}/\text{psi}$ or -0.81%. At 15.38 psia, the thermal energy correction reduces to -0.383%. Since the thermal energy correction is approximately equal to the kinetic energy correction in the region where the corrections are large, it was assumed that the corrections cancelled each other and were not applied to the experimental data points. The experimental apparatus was deliberately operated so that the corrections would cancel each other in the low pressure region. The flow rates ranged between 3.31 and 11.5 pounds per hour.

VI. CALCULATIONS

The Joule-Thomson coefficients, $(\Delta T/\Delta P)_H$, were computed by approximating the differential changes in temperature and pressure with small finite changes. These changes were limited to a maximum of 1.5°F and 8.6 psi and they were measured directly. Changes in temperature were measured by differential thermocouples and changes in pressure were measured by a differential mercury manometer.

The temperature and pressure of each Joule-Thomson coefficient was determined by the arithmetical mean of the inlet and exhaust values. The temperature of the gas at the inlet of the calorimeter was measured by a platinum-resistance thermometer. The inlet pressure was measured by a mercury manometer when below three atmospheres absolute. The laboratory pressure balance [40] was used to measure the inlet pressure when above three atmospheres. The exhaust temperature and pressure of the gas were computed from the inlet values minus the change in value due to throttling. Calibration and corrections to the temperature-measuring devices are covered in Appendix I. Pressure information is given in Appendix II.

Corrections to the measured Joule-Thomson coefficients due to thermal transfer and kinetic energy changes were calculated previously (see Thermodynamic Analysis). These corrections were found to be less than 0.8 percent and essentially equal in magnitude. Neither correction was applied to the measurements since they tended to cancel each other. Therefore all Joule-Thomson coefficients were calculated by dividing the measured temperature change by the measured pressure change.

Unfortunately the ease of calculating a single Joule-Thomson coefficient was complicated by relating several coefficients to the same isotherm. The temperature of each coefficient was related to the measured temperature change. This change could only be estimated for a particular pressure change prior to the measurement. It was not feasible to constantly adjust the temperature and pressure to obtain the desired values since the equipment was operated with a single pass of the gas. Therefore the resulting temperature of the coefficient never fell on a particular isotherm but only in the close vicinity. A small temperature correction was necessary to place a data point on the nearest isotherm. This correction was usually less than 0.2°F. It was obtained graphically from a rough temperature versus Joule-Thomson coefficient plot.

Since the 100°F isotherm for n-butane did not plot as a straight line, a correction was made for the difference between the experimentally measured integral and the desired differential Joule-Thomson coefficient resulting from the finite pressure change. The experimental data points were fitted to an equation of the form,

$$\bar{\mu} = a' + b'P + c'P^2 \quad (15)$$

where the constants a' , b' and c' were determined by a least-squares fit and

$$\bar{\mu} \equiv \frac{\int_{P_1}^{P_2} \mu dP}{\int_{P_1}^{P_2} dP} = \Delta T / \Delta P \quad (16)$$

Results of the curve-fit are given in Table 3 and numerical values of a' , b' and c' are given in Table 5.

It was assumed that the desired 100^oF isotherm of differential coefficients would fit an equation similar to Equation (15):

$$\mu \equiv (\partial T/\partial P)_H = a + bP + cP^2 . \quad (17)$$

Upon substituting μ of Equation (17) into Equation (16) and integrating between the inlet pressure P_1 and the exhaust pressure P_2 , the following relationship for $\bar{\mu}$ was found

$$\begin{aligned} \bar{\mu} &= \frac{\int_{P_1}^{P_2} (a + bP + cP^2) dP}{\int_{P_1}^{P_2} dP} \\ &= a + (b/2)(P_1 + P_2) + (c/3)(P_1^2 + P_1P_2 + P_2^2) . \end{aligned} \quad (18)$$

Since the pressure of $\bar{\mu}$ was the arithmetical mean of P_1 and P_2 , the differential Joule-Thomson coefficient was determined for this mean pressure by Equation (17):

$$\mu = (\partial T/\partial P)_H = a + b[(P_1 + P_2)/2] + c[(P_1 + P_2)/2]^2 . \quad (19)$$

Using Equations (18) and (19) to determine the difference between $\bar{\mu}$ and μ ,

$$\bar{\mu} - \mu = (c/12)(P_2 - P_1)^2 .$$

For a first approximation of c , the value of c' determined from the

integral data points was used. Differential coefficients were then calculated for each integral coefficient in the 100^oF isotherm by the relationship

$$\mu = \bar{\mu} - (\bar{\mu} - \mu) = \bar{\mu} - (c/12)(P_2 - P_1)^2 .$$

The calculated differential coefficients were then fitted to Equation (17) and a new value of c was determined. The new value of c was 1.090614×10^{-5} and it compared favorably with the value of c' which was 1.092818×10^{-5} ; therefore no further iterations were made. The calculated values of μ and numerical values of a , b , and c are given in Tables 3 and 5, respectively.

VII. ERROR ANALYSIS

Error in the values of the Joule-Thomson coefficients was directly related to the accuracy of the temperature and pressure measurements. Equipment limitations and non-isenthalpic conditions were the primary cause of error in both the absolute value and relative change in temperature and pressure values.

In Appendix I, error in the measurement of the Joule-Thomson temperature due to instrumentation inaccuracies was calculated to be less than 0.052°F . A change of 0.052°F in the temperature of the coefficient could result in a difference of 0.03 percent in the Joule-Thomson value. Error in the thermocouple readings used in the calculation of the temperature change of the Joule-Thomson expansion was found to be less than 0.30 microvolt. Since the smallest thermocouple reading was larger than 40 microvolts, the error in thermocouple measurements would cause an error of less than 0.7 percent in the Joule-Thomson values.

In Appendix II, errors in the absolute pressure and the pressure change used in the calculation of the Joule-Thomson coefficients were estimated to be less than 0.1 psi and 0.05 mm Hg, respectively. A pressure error of 0.1 psi would cause a maximum difference of 0.03 percent in the Joule-Thomson coefficients. Since the smallest pressure change was 125 mm Hg, an error of 0.05 mm Hg would result in a maximum error of 0.04 percent in the Joule-Thomson values.

Fluctuations in the pressure and pressure change due to the controlling manostat were less than 0.1 mm Hg. A pressure-change fluctuation of 0.1 mm Hg could result in an error of 0.08 percent of the

Joule-Thomson value. Since these fluctuations could cause a Joule effect of the same magnitude to be superimposed on the Joule-Thomson fluctuation, the 0.1 mm Hg pressure fluctuation might induce an error of 0.16 percent of the Joule-Thomson coefficient.

The errors in the Joule-Thomson coefficient due to thermal transfer and kinetic energy changes were previously calculated (see Thermodynamic Analysis) to be less than 0.8 percent of the Joule-Thomson values. They were approximately equal in value and tended to cancel each other. An error of less than 0.4 percent was assumed by cancelling the thermal transfer with the kinetic energy change.

Impurities in the propane and n-butane used in this study were determined by chromatographic analysis and listed in Table 9. The purity of the propane and n-butane was found to be 99.91 and 99.66 mol percent, respectively. Closely related hydrocarbons composed the major impurities. Based on the results of the Joule-Thomson coefficient of mixtures of methane-ethane and methane-n-butane by Sage [32,33] and nitrogen-ethane by Stockett and Wenzel [41], an error of less than 0.1 percent of the Joule-Thomson value was attributed to impurities.

The weight rate of flow through the porous thimble was determined by weighing the storage cylinders before and after each experimental measurement. The estimated error in the weights was approximately five percent. Since the thermal transfer and kinetic energy change which used the weight flow rate were assumed to cancel each other, no additional error was attributed to error in the flow rate through the thimble.

The maximum error in the Joule-Thomson coefficients was determined by adding the individual errors which were:

<u>Source</u>	<u>% Error</u>
Temperature	0.03
Temperature change	0.70
Pressure	0.03
Pressure change	0.04
Pressure fluctuations	0.16
Non-isenthalpic conditions	0.40
Impurities	0.10
	<hr/>
Total	1.46

Therefore the maximum error was less than 1.5 percent of the measured Joule-Thomson coefficient.

VIII. RESULTS

Joule-Thomson measurements were made on gaseous propane at temperatures from 100 to 280^oF and at pressures from 8 to 66 psia. Joule-Thomson measurements were also made on gaseous n-butane at temperatures from 100 to 280^oF and at pressures from 8 to 42 psia. Results of these measurements are given for propane in Table 1 and for n-butane in Table 3. Corrected values of the coefficients, determined by a least-squares fit of the experimental points, are included in these tables. The results are also given in graphical form in Figures 7 through 10. For propane, Figure 7 indicates the relationship between the Joule-Thomson coefficient and pressure at constant temperatures. Figure 8 indicates the Joule-Thomson coefficient versus temperature at constant pressures for propane. For n-butane, Figures 9 and 10 show similar relationships. A temperature interval of 60^oF was used between isotherms. The pressure interval between experimental points varied but usually ranged from 10 to 20 psi.

A differential Joule-Thomson coefficient was assumed to have been measured directly, since small finite changes in temperature and pressure were used. (Other types of Joule-Thomson coefficients are "integral" and "isothermal" which is defined as $(\partial H/\partial P)_T$.) Temperature changes of 1.0^oF and pressure changes from 3 to 8 psi were typical. The pressure listed for each coefficient was the arithmetical mean of the inlet and exhaust pressures of the calorimeter. For example, a Joule-Thomson coefficient listed at 8 psia might have been measured with an inlet pressure of 12 psia and an exhaust pressure of

4 psia. Each isotherm of Joule-Thomson coefficients in Figures 7 and 9 is experimentally valid from the lowest exhaust pressure to the highest inlet pressure. The limits of the experimental range are indicated by the solid lines in the above figures.

All of the measured Joule-Thomson coefficients were positive and increased in value with increasing pressure and molecular weight. The coefficients decreased in value with increasing temperature. Each listed Joule-Thomson coefficient in Tables 1 and 3 is the result of approximately 10 individual points taken during the approach to steady state over a time period ranging from 4 to 10 hours. Most of the points during the approach to steady state were taken at thirty-minute intervals starting about two hours after the start of the throttling process. Figure 13 indicates the individual points from which one point in Table 3 is composed. An experimental measurement was terminated when the difference in the ratio of ΔT to ΔP for five consecutive points was less than 0.3 percent.

Previous calculations (see Error Analysis) indicated the measurements to have a maximum error of less than 1.5 percent. No point, after being corrected for temperature, deviated from its isotherm by more than 1.04 percent. Figures 7 and 9 compare the results of this study with previous measurements for propane [28] and n-butane [29], respectively. For propane, the agreement was within 5 percent over the duplicated range. The results for n-butane disagreed to a larger but varying extent. The greatest difference occurred when extrapolating the data to zero pressure. Values of the zero pressure Joule-Thomson coefficient for the present and previous studies for n-butane

on the 100°F isotherm were 0.2563°F/psi and 0.1952°F/psi, respectively. This is a difference of approximately 26 percent. A very definite trend was detectable between the present and previous n-butane coefficients. Agreement improved with increasing temperature and pressure. This trend is a possible clue as to the reason for the discrepancy.

In the earlier study, a constant-volume cam pump was used as the pressure source for all measurements. This pump had a small weight rate of flow near atmospheric pressure and no correction was made to the data for thermal transfer. It was previously shown (see Thermodynamic Analysis) that the error in experimental Joule-Thomson coefficients resulting from thermal transfer can be expressed by

$$C_{\dot{Q}} = \dot{Q} / (\dot{m} C_p \Delta P) = (K_1 \mu) / (\dot{m} C_p) \quad (8)$$

where $K_1 = k A_o (\Delta \theta / \Delta y)_{y_o}$. Application of this correction for thermal transfer to the n-butane data of the previous study would improve the agreement with the present study. However, the lack of flow rate data from the previous study prevented the straightforward use of Equation (8). An estimate of the heat transfer correction was obtained in the following manner. It was observed in the laboratory logbook that all the previous data were measured at a pressure change of approximately 1.0 psi. A pressure change of 1.0 psi would result in a certain volumetric flow rate which is almost independent of the fluid density. This is evident from Darcy's law [42] which can be expressed

$$V' = \epsilon A (\Delta P / \Delta x)$$

where V' is the volumetric flow rate, ϵ the permeability of the

porous material and $\Delta P/\Delta x$ the pressure gradient. Therefore it was assumed that the volumetric flow rate was constant for all previous n-butane measurements.

For an ideal gas, the relation between the mass and volumetric flow rate is

$$\dot{m} = V'\rho = V'P/RT \quad (20)$$

where ρ is the gas density and R the gas constant. Substituting Equation (20) into Equation (8), the following relationship was obtained:

$$C_Q = (K_1 RT \mu) / (V' C_p P) \quad (21)$$

To further simplify Equation (21), changes in gas properties due to thermal effects were assumed to change in a constant ratio. Therefore Equation (21) can be expressed by

$$C_Q = C_1 \mu / P$$

where $C_1 = K_1 RT / V' C_p$.

To obtain a value for C_1 it was further assumed the primary reason for the differences between the Joule-Thomson coefficients for n-butane of the two studies was thermal energy transfer. In particular a value of C_1 was chosen to cause perfect agreement between the Joule-Thomson coefficients of the two studies at 160°F and 14.7 psia. The value calculated for C_1 was 1.79 psi. Using this value, a correction was made to all n-butane values. Results of these

corrections are given in Table 12 and Figure 14. All of the corrected Joule-Thomson values, except those of the 220^oF isotherm, then agreed with the present study. If the experimental values of the 220^oF were multiplied by 1.105 prior to the application of the correction, excellent agreement with this isotherm would have been obtained. This additional correction of 1.105 could have been caused by an error in the pressure change of exactly 0.100 psi or a bath temperature of 120.00^oF instead of 220^oF. Anything which would affect the $\Delta T/\Delta P$ by 1.105 is possible. No single correction which might result from experimental error was found that would correct the 220^oF isotherm without using the thermal-transfer correction.

A similar correction was not applied to the previous propane values because the original data points were observed at considerably higher pressures. The two-phase region for n-butane at 100^oF starts at 51.4 psia. Therefore all experimental points were taken between 14.8 and 50 psia. For propane, twelve of the fifteen original data points were taken between 50 and 550 psia. Since the smoothed data reflected the influence of the higher pressures where the thermal-transfer correction would be small, a correction was not attempted. It was observed that if the previous propane data were extrapolated from the high-pressure region towards zero pressure by a straight line, better agreement between the two studies would be obtained.

Since no other experimentally measured values of the Joule-Thomson coefficient for propane or n-butane were found, values were calculated from other p-v-t data. One value of the Joule-Thomson

coefficient for propane at 50 psia and 200^oF was calculated from an experimental isothermal throttling coefficient and heat capacity given in a recent paper [43]. This value was compared to an equivalent value from this study and also the previous propane study. The results of this comparison were 0.1154, 0.1158 and 0.1165^oF/psi, respectively.

Joule-Thomson coefficients were calculated from the Benedict-Webb-Rubin equation [11] with its original coefficients. Derivation of the equation used to calculate the coefficients is given by Ahlert and Wenzel [44] and consisted of the straightforward but lengthy procedure of substituting the B-W-R equation into Equation (2). Results of the calculations for propane and n-butane are listed in Table 7. A comparison of the calculated coefficients with the coefficients of this study and also the previous study are given in Figures 7 and 9. The calculated coefficients from the B-W-R equation were larger in value than the equivalent coefficients of this study. All isotherms of the Joule-Thomson coefficients for both propane and n-butane, except the 220^oF n-butane isotherm of the previous study, indicated the same general trends. This 220^oF isotherm was lower in value than anticipated for all pressures.

Since the greatest difference in the Joule-Thomson coefficients of the experimental studies occurred when extrapolated to zero pressure, a comparison with other p-v-t data was made at attenuation. McGlashan and Potter [45] experimentally measured the second virial coefficients of six alkanes from propane to n-octane. They expressed their results by the following empirical equation:

$$B/V_c = 0.430 - 0.886(T_c/T) - 0.694(T_c/T)^2 - 0.0375(n-1)(T_c/T)^{4.5} \quad (20)$$

where B is the second virial coefficient, V_c the critical volume, T_c the critical temperature and n the number of carbon atoms. Second virial coefficients calculated from this equation were compared with second virial coefficients calculated from experimental p-v-t data on methane through n-octane of numerous authors. For propane and n-butane the p-v-t data of seven different studies were used [46,47,48,49,50,51, 52]. The results of this comparison were given in graphical form by McGlashan and Potter [45]. Unfortunately no tabular results were given but a visual inspection of the graphs indicated the empirical equation to yield values of the second virial coefficients which favorably agreed with those calculated from the p-v-t data. In the 100 to 280°F range second virial coefficients calculated from the p-v-t data were slightly larger (smaller negative values) than those calculated from the empirical equation. The deviation increased with molecular weight from about one percent for propane to approximately ten percent for n-hexane. For n-butane, second virial coefficients calculated from the empirical equation were too small by approximately two percent.

At low pressures the second virial coefficient is related to the Joule-Thomson coefficient by the following equation:

$$\mu = C_p^{-1}(T(\partial B/\partial T)_P - B) \quad (21)$$

Substituting Equation (20) into Equation (21), Francis and Luckhurst [12] obtained the following equation for calculating zero pressure Joule-Thomson coefficients:

$$\mu^o = (V_c/C_p^o)(0.2063(n-1)(T_c/T)^{4.5} + 2.082(T_c/T)^2 + 1.772(T_c/T) - 0.430$$

where the superscript "o" refers to zero pressure. They compared Joule-Thomson coefficients calculated from this equation to experimental Joule-Thomson coefficients. The comparisons indicated the above equation yielded Joule-Thomson coefficients which agreed with other experimentally measured Joule-Thomson coefficients, both hydrocarbon and inorganic, except for the propane and n-butane coefficients of the previous study. Zero pressure Joule-Thomson coefficients from this study compared favorably with the above equation. The results of these comparisons are given in Table 6 and Figures 11 and 12. The comparison indicated a maximum difference of 1.5 percent for propane and 2.8 percent for n-butane. The differences are in the proper direction to agree with the p-v-t data for propane and n-butane [46 through 52] which McGlashan and Potter used to compare with their empirical equation.

The Joule-Thomson apparatus used in this study was built from the experience gained from two previous Joule-Thomson studies [28,36] and considerable laboratory testing. A detailed description of the equipment has been given (see Experimental Apparatus). The most significant difference between this and other Joule-Thomson apparatus was the high weight rate of flow below atmospheric pressure. The high flow rate reduced the error due to thermal transfer in the low pressure region.

IX. CONCLUSIONS

The measured Joule-Thomson coefficients of this study did not agree with previous experimental values for n-butane, which were shown to be in error. The disagreement increased with decreasing pressure to a maximum of approximately twenty-six percent at zero pressure absolute. When a thermal-transfer correction was applied to the previous values, a satisfactory agreement was obtained except for the 220° isotherm. This isotherm did not conform to the general trends of the other isotherms when compared to the experimental values of this study or calculated values from the Benedict-Webb-Rubin equation. The main value of Joule-Thomson coefficients calculated from the B-W-R equation was to point out inconsistencies in experimental values rather than any claimed accuracy of the calculated coefficients.

If a correction were made to the $\Delta T/\Delta P$ ratio of the 220°F isotherm of the previous study for the type of error that would be caused by inaccuracies in the pressure change, bath temperature, thermocouples, etc., and then the heat-transfer correction applied, the isotherm could be made to agree with this study.

For propane, the agreement between the present and previous studies was acceptable. The high concentration of data points above 50 psia could explain the better agreement. At pressures where the fluid density is appreciable, the thermal transfer correction is small.

Joule-Thomson coefficients calculated at zero pressure absolute from the equation of Francis and Luckhurst [12] agreed within 2.8

percent for both propane and n-butane values of this study. The equation was shown to represent the p-v-t data of various authors on ethane through n-octane within a narrow error band. The excellent agreement at zero pressure is significant, for the low pressure region is the most difficult in which to measure Joule-Thomson coefficients.

All isotherms of the measured Joule-Thomson coefficients of this study for both propane and n-butane, except the 100^oF n-butane isotherm, are plotted as straight lines. Based on the previous Joule-Thomson measurements and also the B-W-R equation, all isotherms might have some curvature toward higher values at higher pressures. Except for the 100^oF isotherm for n-butane, no curvature was detected at the pressures of this study.

Since the slopes of the isotherms of the previous Joule-Thomson measurements are larger than those of this study, one might expect the data to diverge at higher pressures. If the thermal-transfer correction is applied to the previous values, the slopes are approximately equal. Therefore the data would not diverge.

The improved values of the present study is not only due to instrumentation improvements since 1935 but also to changes in calorimeter design. The most significant improvement was the increased flow through the porous thimble at low pressures. The equations used to relate errors in the values of experimentally measured Joule-Thomson coefficients to the flow rate through the thimble are unique in that the Joule-Thomson coefficient was previously thought to be essentially independent of extensive measurements [53].

X. FUTURE WORK

Two areas of continued study with the present equipment are desirable. First, using the high-pressure vessel not used in this study; an increased pressure range for propane and n-butane would permit a comparison of measurements where all flow rates are high. Second, an increase in the number of hydrocarbons measured would be beneficial to correlations between macroscopic measurements and microscopic properties. Experimental Joule-Thomson data on higher-molecular weight-normal hydrocarbons, isomers, and mixtures are very sparse. Present values for iso-butane [10,54] are significantly lower than the values of n-butane. No experimental Joule-Thomson measurements for any other hydrocarbon isomer were found.

The most beneficial change to the equipment would be to replace the evaporation-condensation single-pass flow with a recirculating pump. This change would permit the determination of several data points per day rather than two per week. A large-capacity diaphragm pump seems most feasible. Several pumps in parallel might be required at low pressures. A metallic diaphragm, or possibly one made of some new miracle polymer material, would be necessary to prevent contamination of the hydrocarbon at high temperatures.

XI. REFERENCES

1. J. H. Potter, "Some Recent Throttling Investigations," Second Symposium on Thermophysical Properties, Princeton, N.J., 1962, pp 83-87.
2. J. O. Hirschfelder, R. B. Ewell and J. R. Roebuck, "Determination of Intermolecular Forces Joule-Thomson Coefficients," J. Chem. Phys. 6, 1938, pp 177A and 205-218.
3. M. Klein, "Determination of Intermolecular Potential Functions from Macroscopic Measurements," J. Research of NBS, A. Physics and Chemistry 70A, 1966, pp 259-269.
4. J. O. Hirschfelder and W. E. Roseveare, "Intermolecular Forces and the Properties of Gases," J. Phys. Chem. 43, 1939, pp 15-35.
5. T. Ishikawa, "Application of the New Equation of State of the Joule-Thomson Effect," Bull. Chem. Soc. Japan 26, 1953, pp 529-531.
6. J. O. Hirschfelder, C. F. Curtis and R. B. Bird, Molecular Theory of Gases and Liquids, John Wiley & Sons, 2nd Printing, 1965, pp 2-3.
7. J. O. Hirschfelder, C. F. Curtis and R. B. Bird, Molecular Theory of Gases and Liquids, John Wiley & Sons, 2nd Printing, 1965, pp 173-177.
8. F. F. Hung, "Determination of Virial Coefficients and Derivatives from Free Expansion Data--with Application to Nitrogen," Proc. 3rd Symp. on Thermophysical Properties, Papers, Lafayette, Ind., 1965, pp 98-103.
9. R. H. Perry, C. H. Chilton and S. D. Kirkpatrick, Perry's Chemical Engineers' Handbook, 4th Ed., McGraw-Hill, New York, 1963, p 3-98.
10. F. S. Manning and L. N. Canjar, "Joule-Thomson and Second Virial Coefficients for Hydrocarbons," J. Chem. Eng. Data 6, 1961, pp 364-365.
11. M. Benedict, G. B. Webb and L. C. Rubin, "An Empirical Equation for Thermodynamic Properties of Light Hydrocarbons and their Mixtures; Constants for Twelve Hydrocarbons," Chem. Eng. Prog. 47, 1951, pp 419-422.
12. P. G. Francis and G. R. Luckhurst, "Joule-Thomson Coefficients and the Principle of Corresponding States," Trans. Faraday Soc. 59, 1963, pp 667-672.

13. J. P. Joule and W. Thomson, "On the Thermal Effects of Fluids in Motion--Part IV," Phil. Tr. Roy. Soc. 152, Part 2, 1862, pp 579-589.
14. J. P. Joule and W. Thomson, "On the Thermal Effects Experienced by Air Rushing through Small Apertures," Phil. Mag. Ser. 4, 4, 1852, pp 481-492.
15. H. L. Johnston and D. White, "VII--A Summary of Experimental Determinations of Joule-Thomson Effects in Gases," Trans. Am. Soc. Mech. Engrs 70, 1948, pp 651-654.
16. F. E. Kester, "The Joule-Thomson Effect in Carbon Dioxide, I. Experimental," Phys. Rev. 21, 1905, pp 260-288.
17. L. G. Hoxton, "The Joule-Thomson Effect for Air at Moderate Temperatures and Pressures," Phys. Rev. 13, 1919, pp 438-479.
18. E. S. Burnett and J. R. Roebuck, "On a Radial Flow Porous Plug and Calorimeter," Phys. Rev. 30, 1910, pp 529-531.
19. E. S. Burnett, "Experimental Study of the Joule-Thomson Effect in Carbon Dioxide," Phys. Rev. 22, 1923, pp 590-616.
20. J. R. Roebuck, "The Joule-Thomson Effect in Air," Proc. Am. Acad. Arts Sci. 60, 1925, pp 537-596; ibid, Vol. 64, 1930, pp 287-334.
21. J. R. Roebuck and H. Osterberg, "Joule-Thomson Effect in Helium," Phys. Rev. 37, 1931, pp 110-111; ibid, Vol. 43, 1933, pp 60-69.
22. J. R. Roebuck and H. Osterberg, "The Joule-Thomson Effect in Argon," Phys. Rev. 46, 1934, pp 785-790.
23. J. R. Roebuck and H. Osterberg, "The Joule-Thomson Effect in Nitrogen," Phys. Rev. 48, 1935, pp 450-457.
24. J. R. Roebuck and H. Osterberg, "The Joule-Thomson Effect in Mixtures of Helium and Nitrogen," J. Am. Chem. Soc. 60, 1938, pp 341-351.
25. J. R. Roebuck and T. A. Murrell, "The Joule-Thomson Effect in Carbon Dioxide," Phys. Rev. 55, 1939, p 240.
26. J. R. Roebuck and H. Osterberg, "The Joule-Thomson Effect in Mixtures of Helium and Argon," J. Chem. Phys. 8, 1940, pp 627-635.
27. J. R. Roebuck, T. A. Murrell and E. E. Miller, "The Joule-Thomson Effect in Carbon Dioxide," J. Am. Chem. Soc. 64, 1942, pp 400-411.

28. B. H. Sage, E. R. Kennedy and W. N. Lacey, "Phase Equilibria in Hydrocarbon Systems; XIII. Joule-Thomson Coefficients of Propane," Ind. Eng. Chem. 28, 1936, pp 601-604.
29. B. H. Sage, E. R. Kennedy and W. N. Lacey, "Phase Equilibria in Hydrocarbon Systems; XIV. Joule-Thomson Coefficients of n-Butane and n-Pentane," Ind. Eng. Chem. 28, 1936, pp 718-720.
30. B. H. Sage, D. C. Webster and W. N. Lacey, "Phase Equilibria in Hydrocarbon Systems; XVIII. Thermodynamic Properties of Ethane," Ind. Eng. Chem. 29, 1937, pp 658-666.
31. B. H. Sage, R. A. Budenholzer and W. N. Lacey, "Phase Equilibria in Hydrocarbon Systems; Joule-Thomson Coefficients of Methane," Ind. Eng. Chem. 31, 1939, pp 369-374.
32. B. H. Sage, R. A. Budenholzer and W. N. Lacey, "Phase Equilibria in Hydrocarbon Systems; Joule-Thomson Coefficient of Gaseous Mixtures of Methane and Ethane," Ind. Eng. Chem. 31, 1939, pp 1288-1292.
33. B. H. Sage, R. A. Budenholzer and W. N. Lacey, "Phase Equilibria in Hydrocarbon Systems; Joule-Thomson Coefficients for Gaseous Mixtures of Methane and n-Butane," Ind. Eng. Chem. 32, 1940, pp 384-387.
34. B. H. Sage, R. A. Budenholzer, D. F. Botkin and W. N. Lacey, "Phase Equilibria in Hydrocarbon Systems; Joule-Thomson Coefficients in the Methane-Propane System," Ind. Eng. Chem. 34, 1942, pp 878-882.
35. B. H. Sage, D. F. Botkin and W. N. Lacey, "Joule-Thomson Coefficients for Two Natural Gases," Trans. Am. Inst. of Mining and Metallurgical Eng. 151, 1943, pp 216-220.
36. H. H. Reamer, G. N. Richter, W. M. DeWitt and B. H. Sage, "Apparatus for the Experimental Study of the Thermodynamic Properties of Water," Trans. ASME 80, 1958, pp 1004-1008.
37. B. H. Sage and W. N. Lacey, Volumetric and Phase Behavior of Hydrocarbons, Gulf Publishing Co., Houston, Texas, 1949, pp 241-245.
38. G. M. Dusinberre, Numerical Analysis of Heat Flow, McGraw-Hill, New York, 1949, pp 52-59.
39. F. D. Rossini, et al., Selected Values of Physical and Thermodynamic Properties of Hydrocarbons and Related Compounds, Carnegie Press, Pittsburgh, Pa., 1953.

40. H. H. Reamer and B. H. Sage, "Experience with Piston-Cylinder Balance for Pressure Measurements," Review of Sci. Instr. 26, 1955, pp 592-593.
41. A. L. Stockett and L. A. Wenzel, "Joule-Thomson Effects for Nitrogen-Ethane Mixtures," A. I. Ch. E. Jour. 10, 1964, pp 557-561.
42. M. Muskat, The Flow of Homogeneous Fluids through Porous Media McGraw-Hill, New York, 1937, pp 55-79.
43. V. F. Yesavage, D. L. Katz and J. E. Powers, "Experimental Determinations of Some Thermal Properties of Propane: Heat Capacity, Joule-Thomson Coefficient, Isothermal Throttling Coefficient and Latent Heat of Vaporization," Proc. 4th Symp. Thermophysical Properties, Papers, College Park, Maryland, 1968, pp 45-53.
44. R. C. Ahlert and L. A. Wenzel, "Joule-Thomson Effects in Gas Mixtures: The Nitrogen-Methane System," A. I. Ch.E. Jour. 15, 1969 pp 256-263.
45. M. L. McGlashan and D. J. B. Potter, "An Apparatus for the Measurement of the Second Virial Coefficients of Some n-Alkanes and of Some Mixtures of n-Alkanes," Proc. Roy. Soc., A, 267, 1962, pp 478-500.
46. J. A. Beattie, W. C. Kay and J. Kaminsky, "The Compressibility of and Equation of State for Gaseous Propane," J. Amer. Chem. Soc. 59 1937, pp 1589-1594.
47. W. W. Deschner and G. G. Brown, "P-V-T Relations for Propane," Ind. Eng. Chem. 32, 1940, pp 836-840.
48. H. H. Reamer, B. H. Sage and W. N. Lacey, "Phase Equilibria in Hydrocarbon Systems--Volumetric Behavior of Propane," Ind. Eng. Chem. 41, 1949, pp 482-484.
49. G. A. Bottomley, D. S. Massie and R. Whytlaw-Gray, "A Comparison of the Compressibilities of Some Gases with that of Nitrogen at Pressures below One Atmosphere," Proc. Roy Soc. 200A, 1949, pp 201-218.
50. F. L. Casado, D. S. Massie and R. Whytlaw-Gray, "The Molecular Weight and Limiting Density of Propane," J. Chem. Soc. 71 1949, pp 1746-1752.
51. C. B. Kretschmer and R. Wiebe, "The Solubility of Propane and the Butanes in Ethanol," J. Amer. Chem. Soc. 73, 1951, pp 3778-3783.

52. J. A. Beattie, G. L. Sinaud and G.-J. Su, "The Compressibility of and an Equation of State for Gaseous Normal Butane," J. Amer. Chem. Soc. 61, 1939, pp 26-27.
53. W. N. Lacey and B. H. Sage, Thermodynamics of One-Component Systems, Academic Press, New York, 1957, p 316.
54. B. H. Sage and W. N. Lacey, Ind. Eng. Chem. 30, 1938, pp 673-681.
55. Amer. Inst. Physics, Temperature, Its Measurement and Control in Science and Industry, 1, 1941, Reinhold, New York, pp 171,174.
56. Amer. Inst. Physics, Temperature, Its Measurement and Control in Science and Industry, 1, 1941, Reinhold, New York, p 169.
57. Amer. Inst. Physics, Temperature, Its Measurement and Control in Science and Industry, 1, 1941, Reinhold, New York, p 304.
58. H. H. Reamer and B. H. Sage, "Performance of a Piston-Cylinder Balance for Pressure Measurements," Rev. Sci. Instr. 40, 1969, pp 183-184.
59. H. H. Reamer and B. H. Sage, "High-Pressure Manometer," Rev. Sci. Instr. 31, pp 337-341.
60. J. H. Perry, Chemical Engineers' Handbook, 2nd Edition, McGraw-Hill, New York, 1941, pp 781-784.

XII. NOTATION

a	constant in Benedict-Webb-Rubin equation
a	constant in manganin-coil calibration equation
a	constant in thermocouple calibration equation
a'	constant in thermal transfer equation
A_0	constant in Benedict-Webb-Rubin equation
A_0	area of lower surface of porous thimble mounting disc enclosed by porous thimble
A_1	cross-sectional area between adjacent radiation shields exterior to thimble
A_2	cross-sectional area between adjacent radiation shields interior to thimble
b	constant in Benedict-Webb-Rubin equation
b	constant in manganin-coil calibration equation
b	constant in thermocouple calibration equation
b'	constant in thermal transfer equation
B	second virial coefficient
B_0	constant in Benedict-Webb-Rubin equation
B-W-R	abbreviation for Benedict-Webb-Rubin
c	constant in Benedict-Webb-Rubin equation
c	constant in thermocouple calibration equation
c'	constant in thermal transfer equation
C	correction factor when used with K.E. or \dot{Q}
C_0	constant in Benedict-Webb-Rubin equation
C_p	heat capacity at constant pressure
C_p^0	heat capacity at zero pressure

d()	symbol for total derivative
EMF	electromotive force
g	gravity
g_c	gravitational constant
H	enthalpy
Hg	symbol for mercury
J-T	abbreviation for Joule-Thomson
k	thermal conductivity of thimble mounting disc
K.E.	abbreviation for kinetic energy
\dot{m}	mass (weight) flow rate
NBS	National Bureau of Standards
mm	millimeter
n	number of carbon atoms in hydrocarbon
n-	normal or straight chain hydrocarbon
P	absolute pressure
P.E.	potential energy
p-v-t	pressure-volume-temperature
\dot{Q}	heat transfer in BTU's per unit of time
Q'	heat transfer in BTU's per pound of fluid
R	gas constant
R_o	resistance of platinum thermometer at ice point
R_t	resistance of platinum thermometer at $t^{\circ}\text{C}$
T	absolute temperature, $^{\circ}\text{R}$
t	temperature in $^{\circ}\text{C}$ or $^{\circ}\text{F}$
T_c	critical temperature, $^{\circ}\text{R}$

u_1	average velocity of gas in calorimeter upstream of the porous thimble
u_2	average velocity of gas in calorimeter downstream of the porous thimble
V	specific volume
V'	volumetric flow rate
V_c	critical specific volume
W'_s	shaft work per pound of fluid
x_i	composition of "i" component
y_o	surface A_o
α	constant in platinum thermometer calibration equation
α	constant in Benedict-Webb-Rubin equation
γ	constant in Benedict-Webb-Rubin equation
δ	constant in platinum thermometer calibration equation
$\partial()$	partial derivative
$\Delta()$	finite difference
μ	symbol of Joule-Thomson coefficient
μ^o	symbol for zero pressure Joule-Thomson coefficient
\emptyset	dimensionless temperature defined by $(T-T_1)/(T_2-T_1)$

XIII. TABLES

Table 1

EXPERIMENTAL JOULE-THOMSON VALUES FOR PROPANE

Pressure (psia)	Experimental J-T Coefficients (°F/psi)	Corrected J-T Coefficient by Least-Squares Fit (°F/psi)	Deviation (%)
100°F			
9.08	0.17983	0.18043	-0.33
9.18	0.17967	0.18046	-0.44
17.75	0.18257	0.18293	-0.20
17.93	0.18319	0.18298	+0.11
24.06	0.18620	0.18472	+0.80
39.11	0.18999	0.18907	+0.49
64.93	0.19701	0.19650	+0.26
66.15	0.19550	0.19685	-0.69
160°F			
8.81	0.13281	0.13341	-0.45
9.16	0.13306	0.13347	-0.31
18.14	0.13490	0.13501	-0.08
18.22	0.13593	0.13502	+0.67
39.62	0.13940	0.13868	+0.52
66.35	0.14274	0.14325	-0.36

Table 1 - Continued

Pressure (psia)	Experimental J-T Coefficients (°F/psi)	Corrected J-T Coefficient by Least-Squares Fit (°F/psi)	Deviation (%)
220°F			
8.26	0.10161	0.10178	-0.17
8.95	0.10198	0.10186	+0.12
28.04	0.10326	0.10393	-0.64
38.90	0.10620	0.10511	+1.04
64.35	0.10752	0.10788	-0.33
280°F			
8.01	0.07958	0.07986	-0.35
15.38	0.08074	0.08039	+0.45
40.93	0.08218	0.08225	-0.08
63.45	0.08389	0.08389	0.00

Table 2

CORRECTED JOULE-THOMSON VALUES FOR PROPANE
BY LEAST-SQUARES FIT

Pressure (psia)	Corrected J-T Coefficient (°F/psi)
100°F	
0	0.17782
10	0.18070
20	0.18358
30	0.18645
40	0.18933
50	0.19220
60	0.19508
70	0.19795
160°F	
0	0.13190
10	0.13361
20	0.13532
30	0.13704
40	0.13875
50	0.14046
60	0.14217
70	0.14388

Table 2 - Continued

Pressure (psia)	Corrected J-T Coefficient (°F/psi)
	220°F
0	0.10089
10	0.10197
20	0.10306
30	0.10415
40	0.10523
50	0.10632
60	0.10740
70	0.10849
	280°F
0	0.07928
10	0.08000
20	0.08073
30	0.08146
40	0.08219
50	0.08291
60	0.08364
70	0.08437

Table 3

EXPERIMENTAL JOULE-THOMSON VALUES FOR n-BUTANE

Pressure (psia)	Experimental Integral* J-T Coeff $\bar{\mu}$ (°F/psi)	Corrected Integral* J-T Coeff $\bar{\mu}$ by L-S Fit (°F/psi)	Calculated Differential J-T Coeff $\bar{\mu}$ (°F/psi)	Corrected Differential J-T Coeff $\bar{\mu}$ by L-S Fit (°F/psi)	Deviation Uncorrected to Corrected Differential J-T Coeff (%)
	100°F				
7.72	.26053	.26204	.26049	.26199	-.57
10.23	.26459	.26416	.26454	.26411	+ .16
12.08	.26730	.26582	.26726	.26578	+ .56
19.29	.27335	.27296	.27332	.27294	+ .14
22.51	.27672	.27653	.27670	.27651	+ .07
26.89	.28075	.28174	.28074	.28173	.00
32.76	.28879	.28939	.28878	.28938	-.21
35.73	.29370	.29354	.29369	.29353	+ .05
41.02	.30186	.30142	.30186	.30141	+ .15

$$* \quad \bar{\mu} = \frac{\int_{P_1}^{P_2} \mu \, dP}{\int_{P_1}^{P_2} dP}$$

Table 3 - Continued

Pressure (psia)	Experimental Differential J-T Coeff (°F/psi)	Corrected Differential J-T coeff (°F/psi)	Deviation (%)
160°F			
9.63	0.18880	0.18868	+ .06
18.67	0.19346	0.19384	- .20
24.79	0.19752	0.19734	+ .09
29.21	0.20002	0.19986	+ .08
39.86	0.20587	0.20595	- .04
220°F			
9.16	0.14183	0.14194	- .08
19.31	0.14586	0.14567	+ .13
27.21	0.14853	0.14856	- .02
40.59	0.15343	0.15347	- .03
280°F			
9.36	0.11014	0.11031	- .15
14.00	0.11123	0.11142	- .17
18.85	0.11312	0.11258	+ .54
30.66	0.11529	0.11541	- .10
40.19	0.11763	0.11769	- .05

Table 4

CORRECTED DIFFERENTIAL JOULE-THOMSON VALUES FOR
n-BUTANE BY LEAST-SQUARES FIT

Pressure (psia)	100°F	J-T Coeff. (°F/psi)
0		0.25630
5		0.25989
10		0.26392
14.7		0.26825
15		0.26854
20		0.27371
25		0.27943
30		0.28569
35		0.29250
40		0.29985
45		0.30774
50		0.31619

Table 4 - Continued

Pressure (psia)	J-T Coeff. (°F/psi)
160°F	
0	0.18318
10	0.18889
14.7	0.19157
20	0.19460
30	0.20032
40	0.20603
50	0.21174
220°F	
0	0.13859
10	0.14225
14.7	0.14398
20	0.14592
30	0.14959
40	0.15326
50	0.15692

Table 4 - Continued

Pressure (psia)	J-T Coeff. (°F/psi)
	280°F
0	0.10807
10	0.11047
14.7	0.11159
20	0.11286
30	0.11525
40	0.11764
50	0.12003

Table 5

EQUATIONS FOR ISOTHERMS

Temperature (°F)	Equation
Propane	
100	$\mu = 0.177823 + .287580 \times 10^{-3}P$
160	$\mu = 0.131902 + .171090 \times 10^{-3}P$
220	$\mu = 0.100888 + .108616 \times 10^{-3}P$
280	$\mu = 0.079275 + .072784 \times 10^{-3}P$
n-Butane	
100	$\bar{\mu} = 0.256366 + .650011 \times 10^{-3}P + .109282 \times 10^{-4} P^2$
100	$\mu = 0.256302 + .652350 \times 10^{-3}P + .109061 \times 10^{-4} P^2$
160	$\mu = 0.183176 + .571298 \times 10^{-3}P$
220	$\mu = 0.138586 + .366743 \times 10^{-3}P$
280	$\mu = 0.108074 + .239157 \times 10^{-3}P$

where μ is expressed in units of °F/psi and P in psia.

Table 6

CALCULATED VALUES OF THE JOULE-THOMSON COEFFICIENT AT ZERO PRESSURE FROM THE EQUATION OF FRANCIS AND LUCKHURST

Temperature (°F)	Calc. Value (°F/psi)	Equivalent Experimental Value (°F/psi)
Propane		
100	0.18046	0.17782
160	0.13326	0.13190
220	0.10192	0.10089
280	0.08020	0.07928
n-Butane		
100	0.26390	0.25630
160	0.18854	0.18318
220	0.14073	0.13859
280	0.10872	0.10807

Table 7

CALCULATED VALUES OF THE JOULE-THOMSON COEFFICIENT FROM
THE BENEDICT-WEBB-RUBIN EQUATION

Pressure (psia)	100°F	160°F	220°F	280°F
Propane				
0	.2064	.1491	.1115	.0859
10	.2079	.1499	.1120	.0862
20	.2095	.1507	.1125	.0865
30	.2112	.1516	.1129	.0867
40	.2130	.1525	.1134	.0870
50	.2148	.1534	.1139	.0873
60	.2168	.1544	.1144	.0876
70	.2188	.1554	.1150	.0879
n-Butane				
0	.2805	.2014	.1499	.1150
10	.2857	.2040	.1513	.1158
20	.2913	.2069	.1529	.1166
30	.2975	.2099	.1544	.1175
40	.3044	.2131	.1561	.1184
50	.3120	.2166	.1579	.1194

Table 8

LABORATORY INSTRUMENTS

Thermocouple measurements

L&N Wenner Potentiometer, Catalog #7559
(Ser. No. 1121093 or Chem. Eng. #20805)

L&N Galvanometer
(Ser. No. 81108 or Chem. Eng. #1254)

L&N Standard Cell, Catalog #100, 1.01923 volts at 24°C
(Ser. No. 768102 or Chem. Eng. #22582)

Platinum resistance thermometer measurements

Temperature measurements

Honeywell Rubicon Resistance Bridge
(Ser. No. B-879 or Chem. Eng. #22687)

L&N Galvanometer, Catalog #2285-B
(Ser. No. 1600861 or Chem. Eng. #22719)

L&N Platinum Resistance Thermometer, Catalog #8163
(Ser. No. 165026 or Chem. Eng. #23446)

Temperature control

L&N Resistance Bridge, Catalog #8067
(Ser. No. 1188897 or Chem. Eng. #20866)

L&N Galvanometer, Catalog #2285-B
(Ser. No. 1165026 or Chem. Eng. #20845)

Caltech Platinum Resistance Thermometer
(Ser. No. 1 or Chem. Eng. #1033)

Temperature calibration

L&N Platinum Resistance Thermometer, Catalog #8163
(Ser. No. 676711 or Chem. Eng. #20121)

Miscellaneous Caltech Designed Instruments

Oil Bath - Chem. Eng. Drawing #27015-XL

Thyratron Modulator - Chem. Eng. Drawing #26533-L

Table 9

RESULTS OF THERMOCOUPLE CALIBRATION*

Temperature (°C)	Thermocouple A (microvolts)	Thermocouple B (microvolts)	Curve-Fit (microvolts)
26.286	1048.70	1048.60	1048.65
36.259	1062.35	1062.50	1062.44
37.716	1523.40	1523.70	1523.55
37.725	1523.70	1523.90	1523.83
54.304	2232.30	2232.40	2232.36
71.083	2971.60	2971.70	2971.95
71.731	3001.00	3001.00	3001.02
86.172	3656.10	3656.10	3655.90
104.383	4504.40	4504.20	4503.92
104.387	4504.00	4504.90	4504.11
121.975	5345.70	5345.30	5345.61
137.640	6112.80	6112.60	6112.74
137.647	6113.60	6113.10	6113.12
0.0	--	--	0.00
20.0	--	--	792.30
40.0	--	--	1692.80
60.0	--	--	2480.92

*The above results must be multiplied by 3 for use with the thermocouple networks of the calorimeter.

Table 9 - Continued

Temperature	Thermocouple A	Thermocouple B	Curve-Fit
80.0	--	--	3374.06
100.0	--	--	4297.63
120.0	--	--	5250.05
140.0	--	--	6229.73

The equation which best fit the data was

$$\mu\text{V} = 0.3870847 \times 10^2 t + 0.459899 \times 10^{-1} t^2 - 0.3311271 \times 10^{-4} t^3$$

where μV is in microvolts and t in $^{\circ}\text{C}$.

Table 10

PLATINUM-RESISTANCE THERMOMETER CALIBRATION

The equation used to correlate all platinum resistance measurements was

$$t = (R_t - R_0) / \alpha R_0 + \delta(t/100 - 1)(t/100)$$

where t is the temperature in $^{\circ}\text{C}$, R_t the resistance in ohms at t $^{\circ}\text{C}$, R_0 the resistance in ohms at 0°C , and α and δ are experimental parameters for a particular thermometer.

The calibration information furnished by NBS for L&N thermometer, Ser. No. 676711:

$$\alpha = 0.0039222_7$$

$$\delta = 1.493_4$$

$$R_0 = 25.530 \quad (25.5304 \text{ measured})$$

The calibration information experimentally determined for L&N thermometer, Ser. No. 165026:

$$\alpha = 0.0039268_5$$

$$\delta = 1.484_6$$

$$R_0 = 25.5535$$

The following measurements were used to establish the calibration of the research thermometer:

NBS Resistance (Ohms)	Temperature ($^{\circ}\text{C}$)	Research Resistance (Ohms)
29.3430	37.723	29.3738
39.2356	137.638	39.2876

Table 10 - Continued

The following resistance measurements were used to check the accuracy of the calibration:

NBS Resistance	32.6956
Calculated Temperature	71.248 ₂₅₉
Research Resistance	32.7334
Calculated Temperature	71.248 ₂₁₂

Table 11

RESULTS OF CHROMATOGRAPHIC ANALYSIS

Substance	Mole %
Propane	
C_2H_6	0.00395
C_3H_6	0.00008
C_3H_8	99.91
1,3- C_4H_8	0.01483
i- C_4H_{10}	0.0606
n- C_4H_{10}	0.00858
n-Butane	
C_3H_8	0.191
i- C_4H_{10}	0.144
CH_4	0.001
C_2H_4	0.001
cis-2- C_4H_{10}	0.003
n- C_4H_{10}	99.66

Table 12

COMPARISON OF JOULE-THOMSON VALUES OF PREVIOUS STUDY
CORRECTED FOR THERMAL TRANSFER WITH VALUES OF THIS STUDY
FOR n-BUTANE

The thermal-transfer correction applied was

$$C_Q = 1.79 \mu/P$$

where μ is the previous Joule-Thomson coefficient and P the absolute pressure.

Pressure (psia)	Previous J-T Coefficient (°F/psi)	Thermally Corrected Value (°F/psi)	J-T Coefficient of this Study (°F/psi)	Deviation (%)
100°F				
14.7	0.2343	0.2628	0.2682	-2.00
20.0	0.2486	0.2708	0.2727	-1.06
40.0	0.3012	0.3146	0.2998	4.93
160°F				
14.7	0.1708	0.1916	0.1916	0.00
20.0	0.1772	0.1931	0.1946	-0.87
40.0	0.1988	0.2077	0.2060	0.82
220°F ($\Delta T/\Delta P$ ratio uncorrected)				
14.7	0.1173	0.1316	0.1441	-8.68
20.0	0.1200	0.1307	0.1459	-10.41
40.0	0.1310	0.1369	0.1533	-10.71
220°F ($\Delta T/\Delta P$ ratio corrected by a factor of 1.105)				
14.7	0.1298	0.1456	0.1441	1.11
20.0	0.1327	0.1446	0.1459	-0.88
40.0	0.1448	0.1513	0.1533	-1.30

XIV. FIGURES

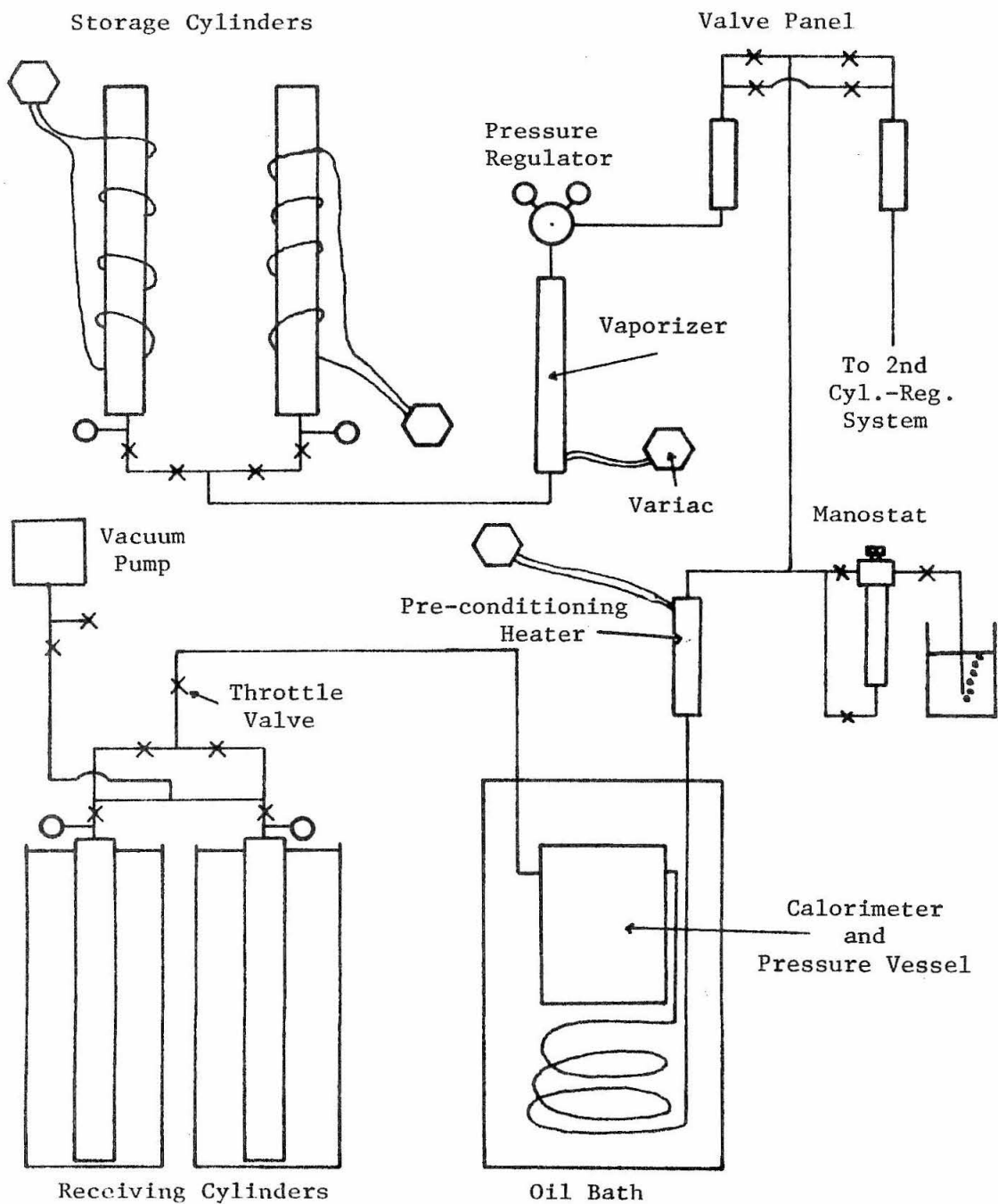


Fig. 1. Schematic diagram of apparatus

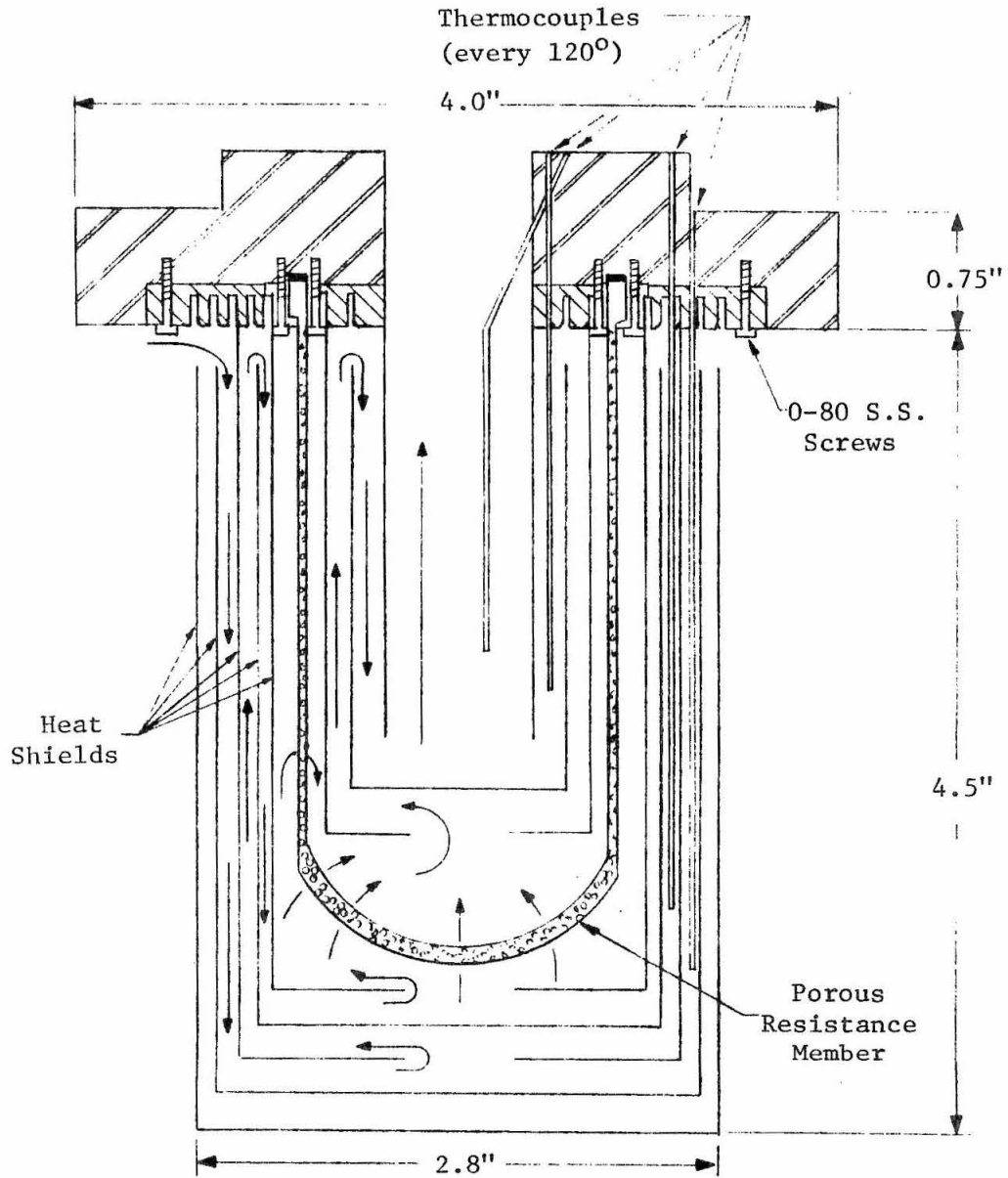


Fig. 2. Full-Scale Drawing of Calorimeter

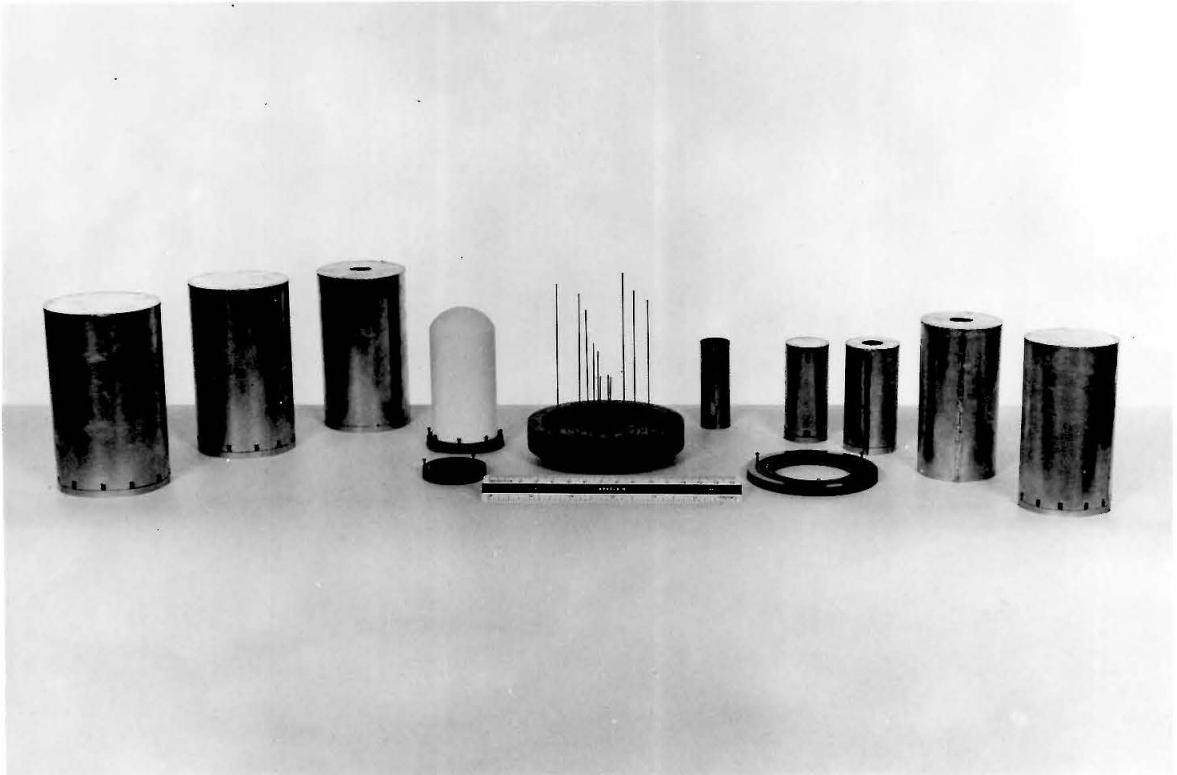


Fig. 3. Photograph of calorimeter showing all components

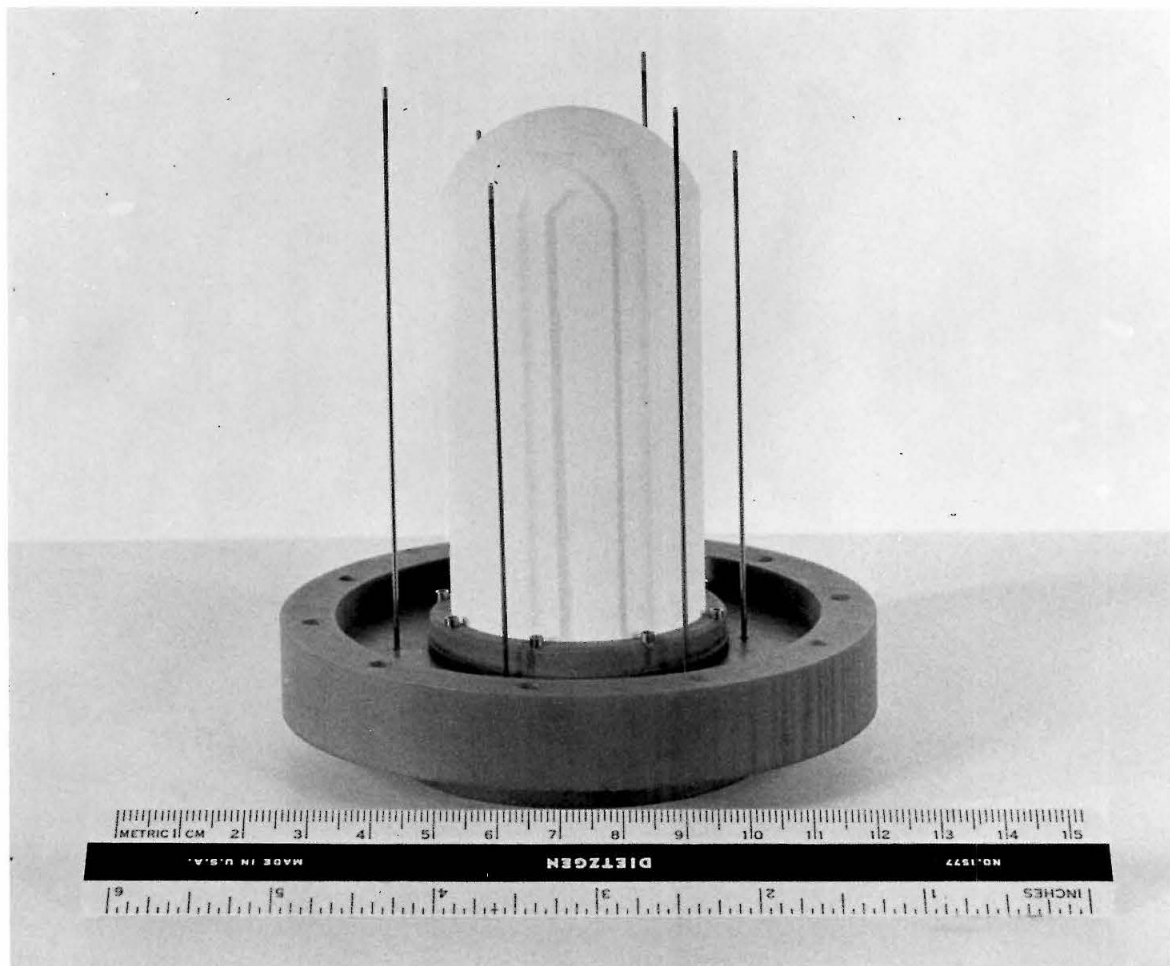


Fig. 4. Photograph of calorimeter with porous thimble installed



Fig. 5. Photograph of calorimeter with radiation-heat shield installed

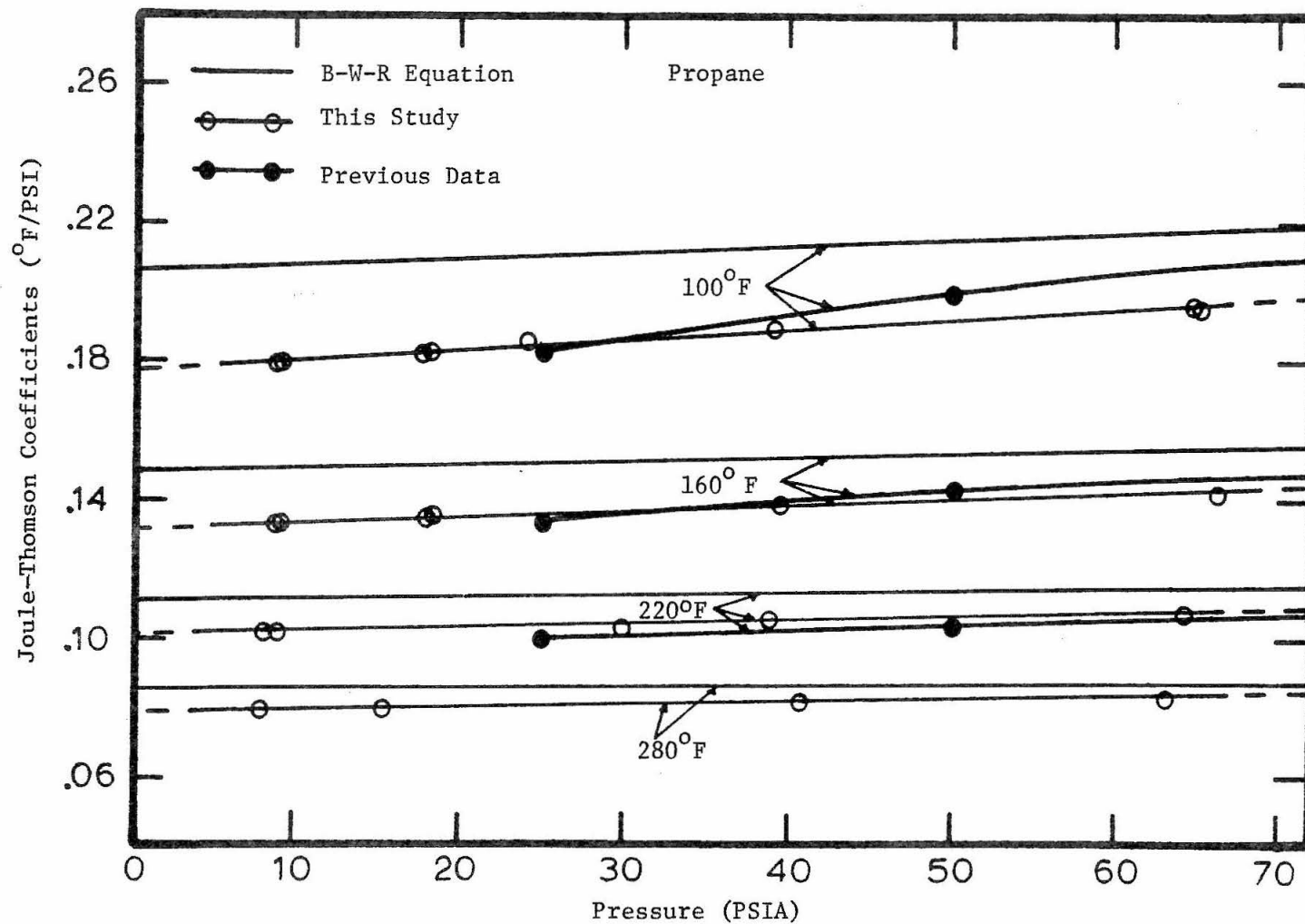


Fig. 7. Joule-Thomson Coefficients versus Pressure at Constant Temperatures

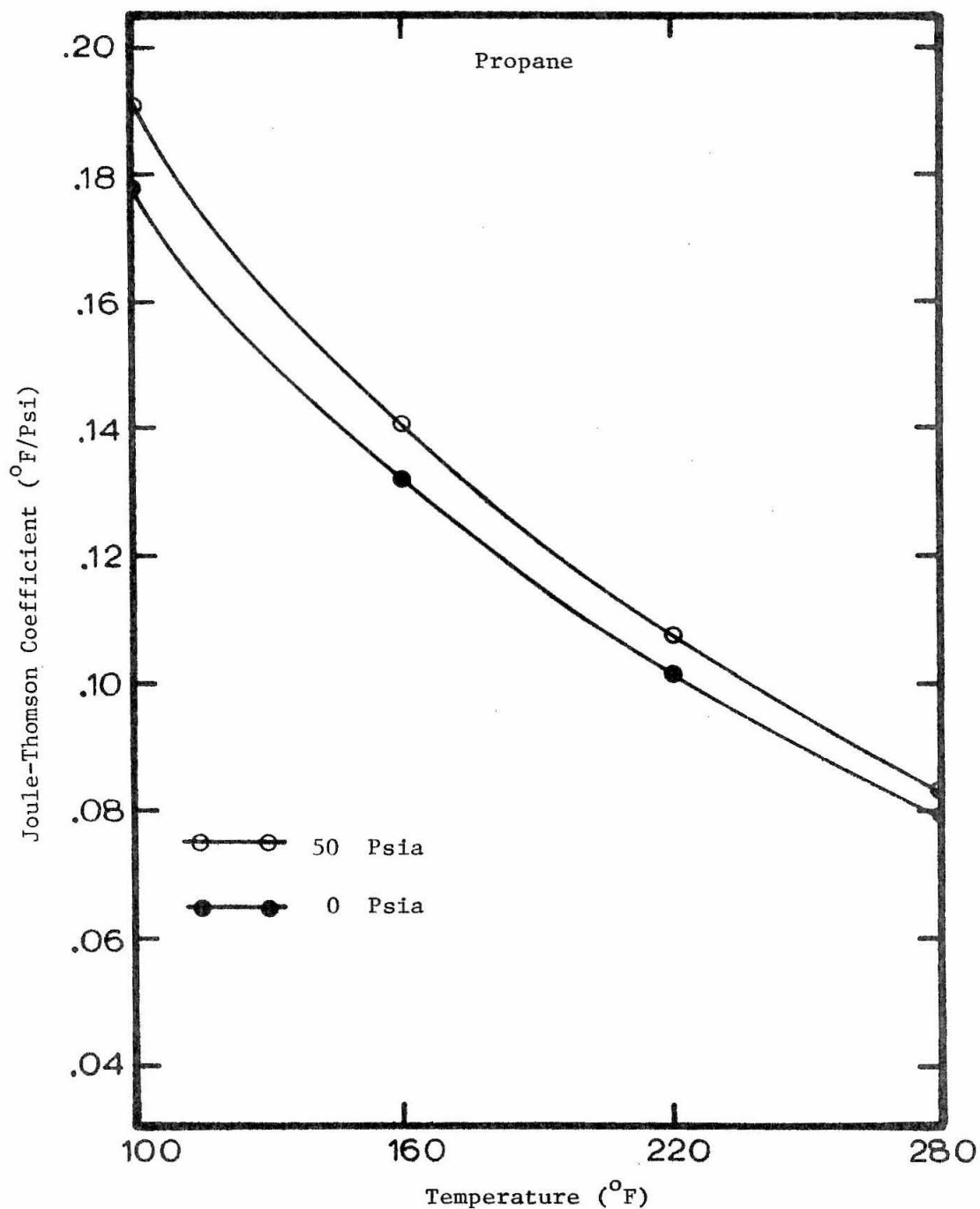


Fig. 8. Joule-Thomson Coefficients vs Temperature at Constant Pressures

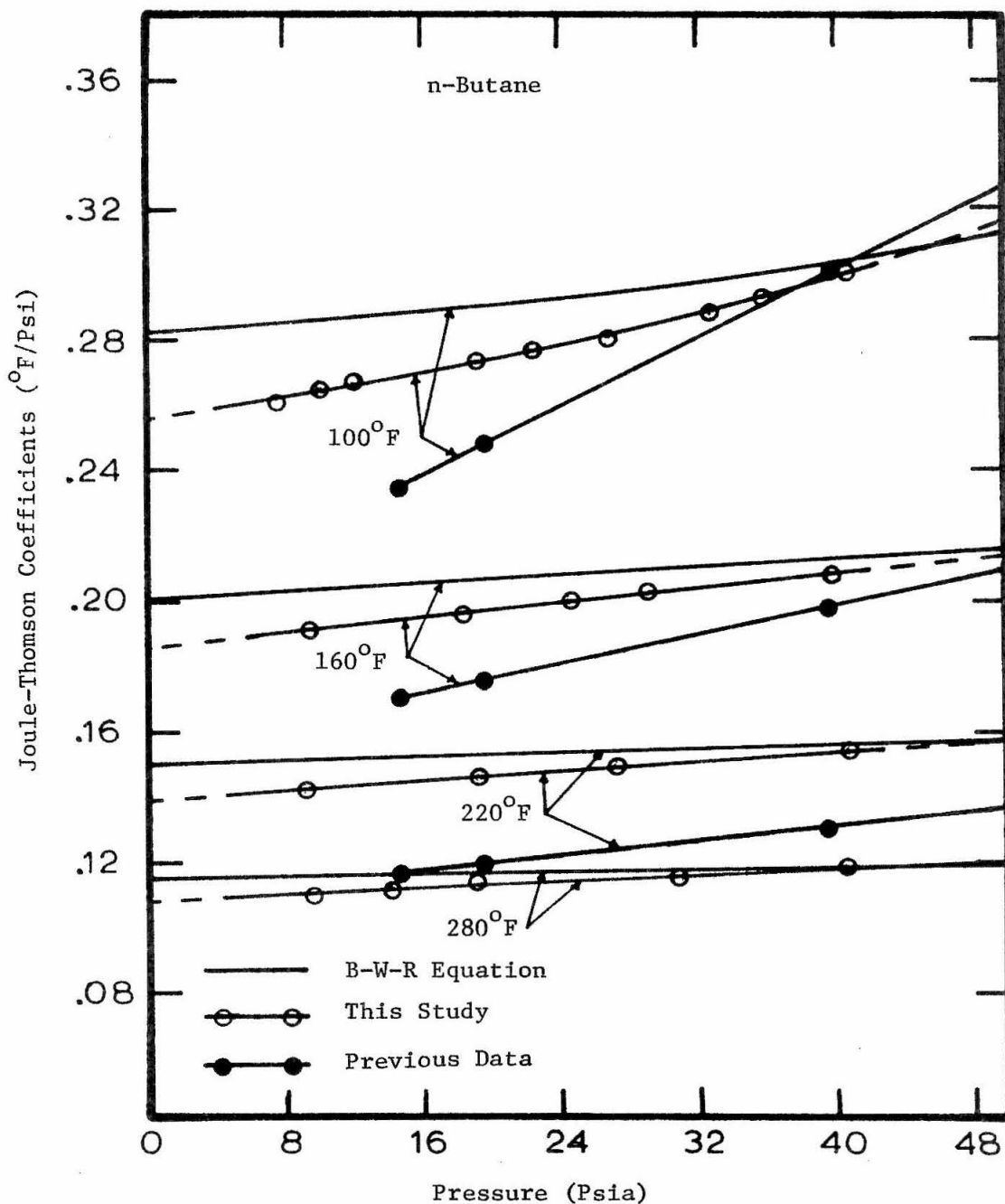


Fig. 9. Joule-Thomson Coefficients of n-Butane vs Pressure at Constant Temperature

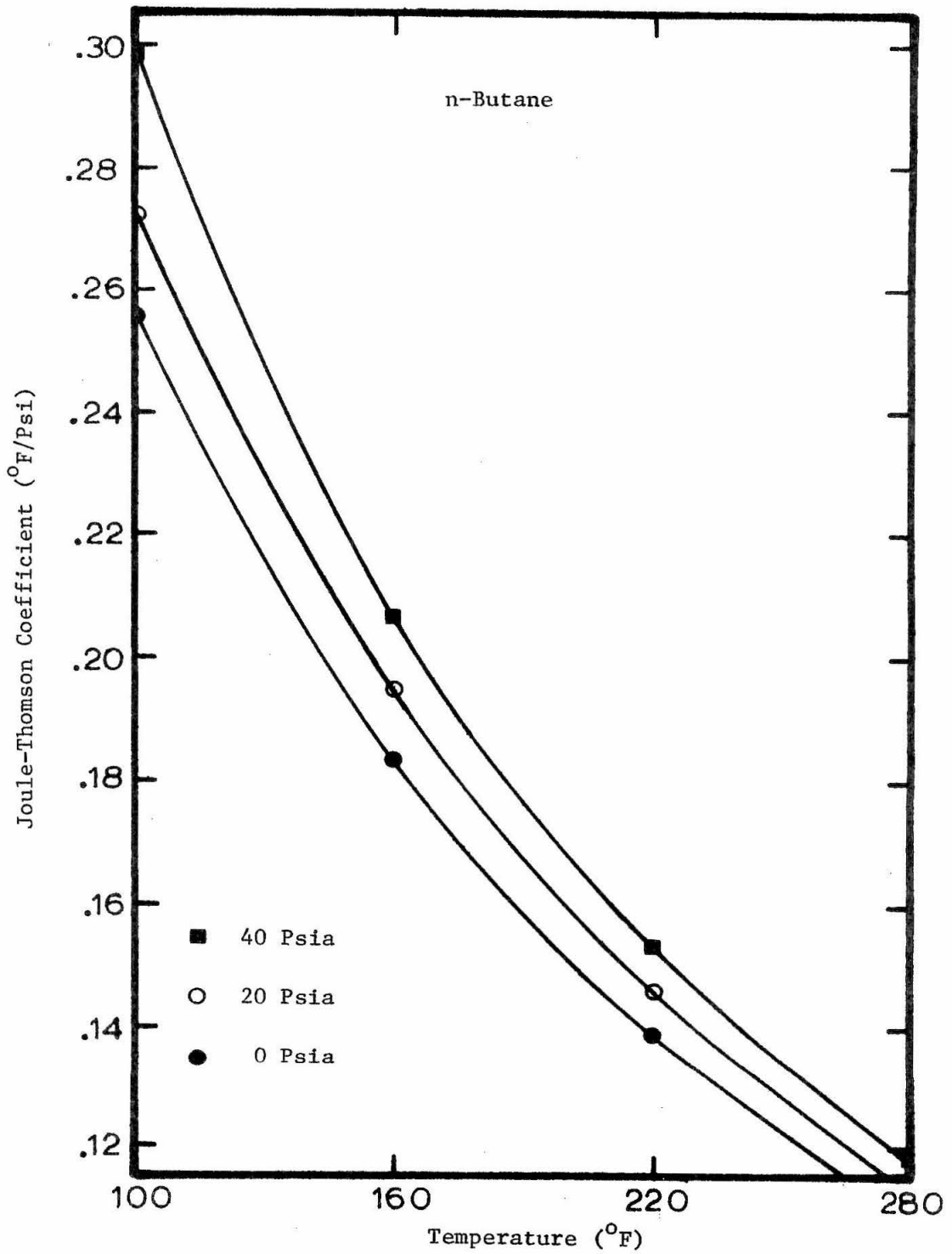


Fig. 10. Joule-Thomson Coefficient vs Temperature at Constant Pressure

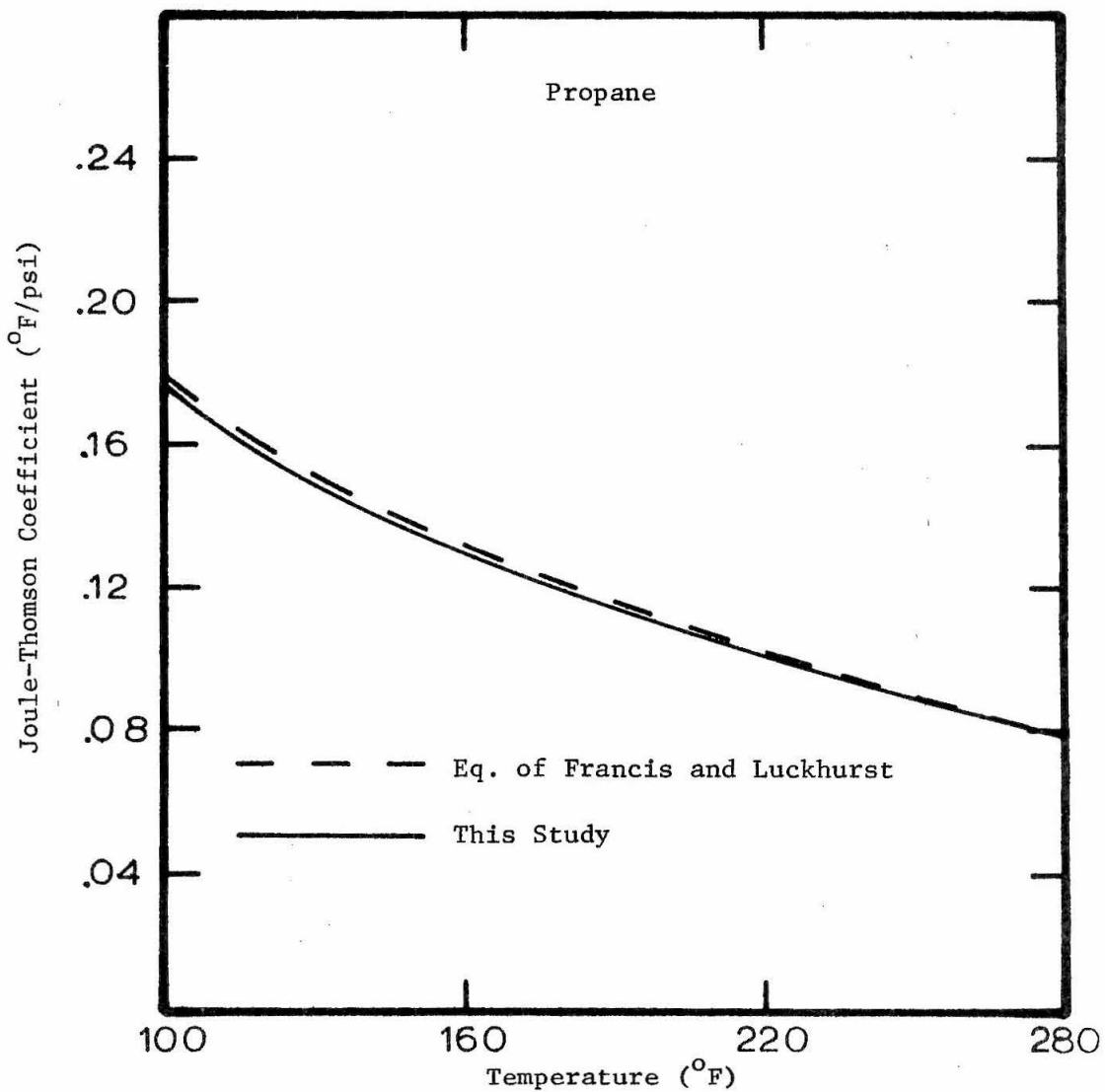


Fig. 11. Comparison of Experimental Joule-Thomson Coefficients for Propane with Equation of Francis and Luckhurst at Zero Pressure

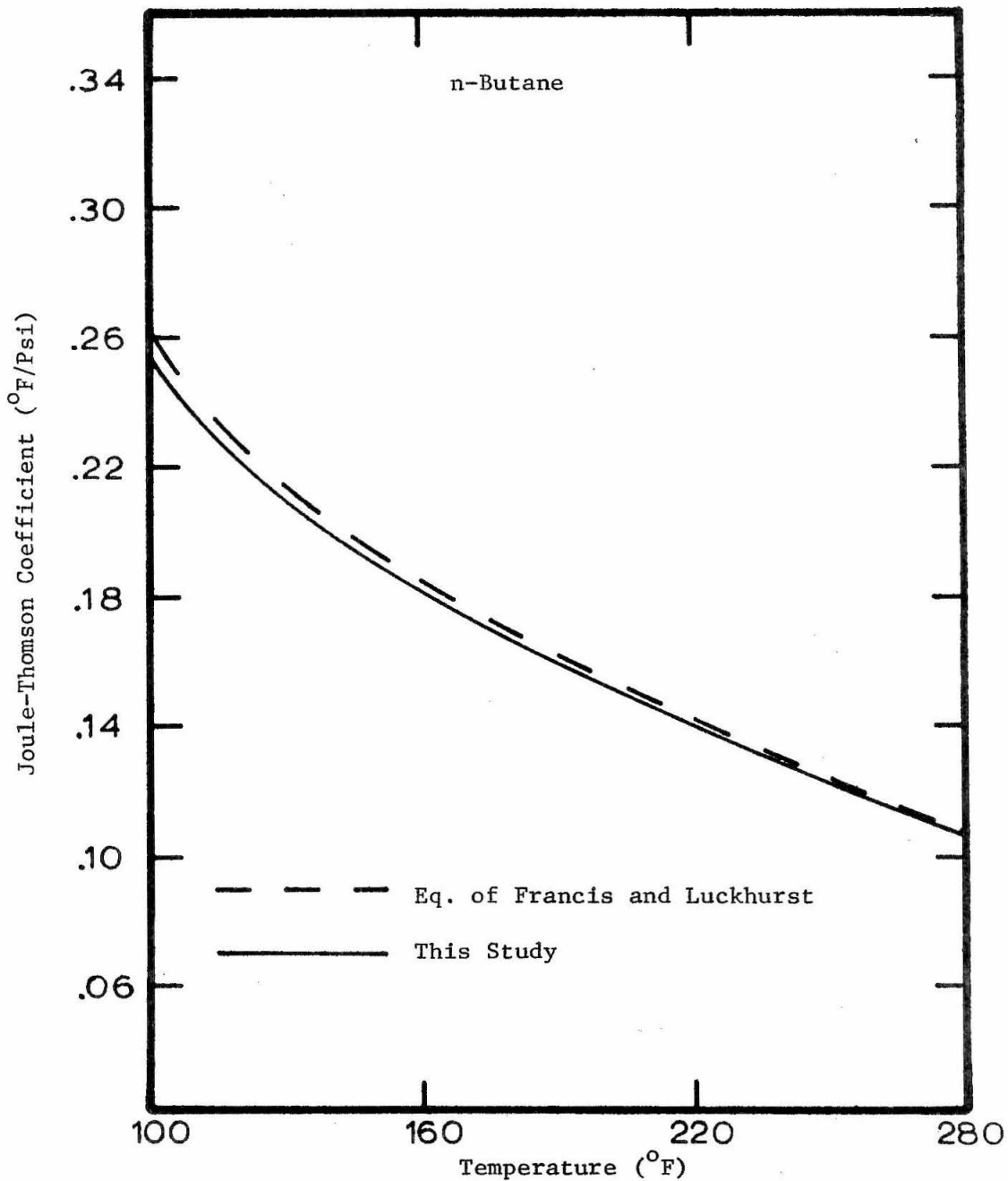


Fig. 12. Comparison of Experimental Joule-Thomson Coefficients for n-Butane with Equation of Francis and Luckhurst

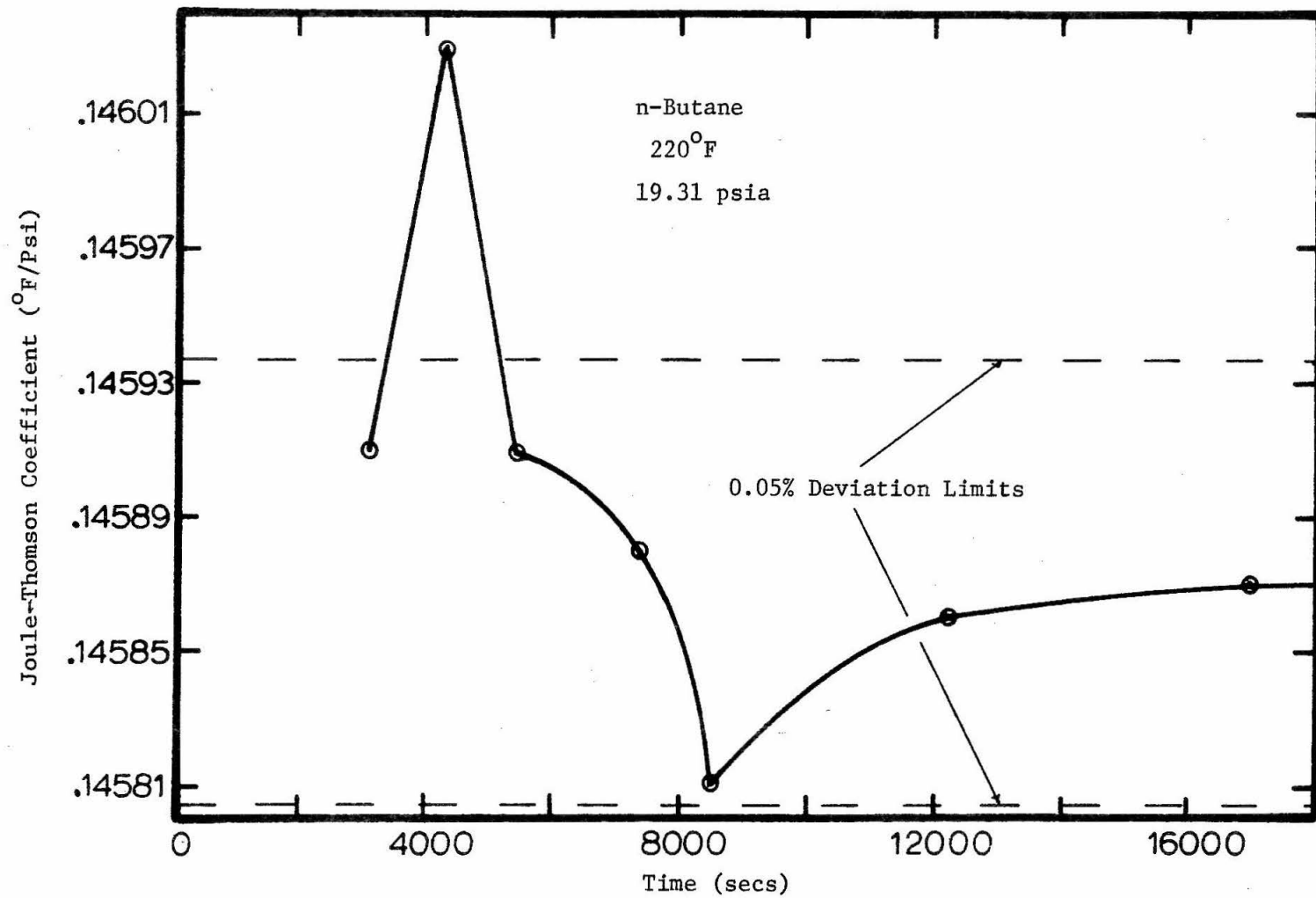


Fig. 13. Measurement of Joule-Thomson Coefficient during Approach to Steady-State

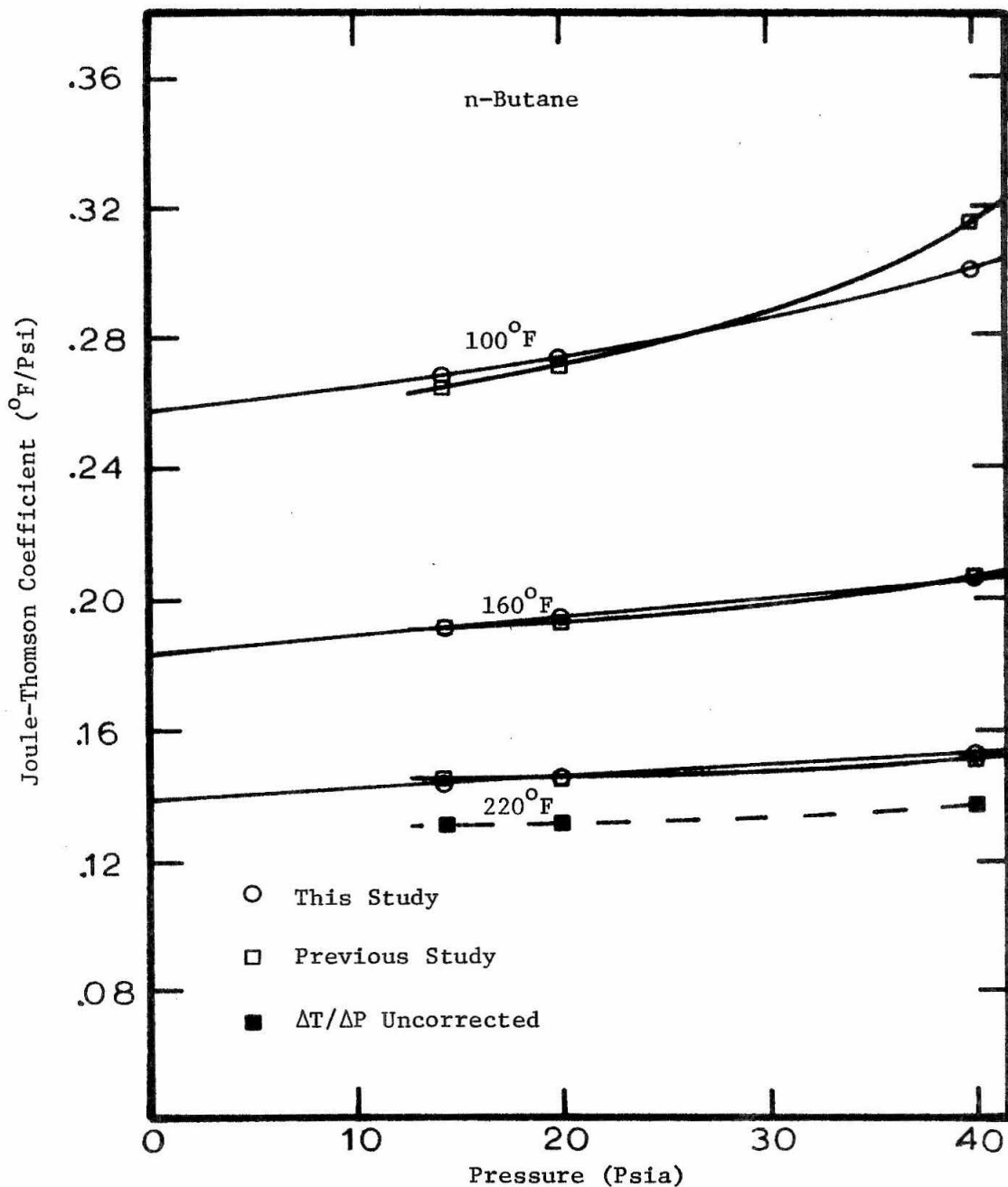


Fig. 14. Comparison of the Joule-Thomson Values of the Previous Study Corrected for Thermal Transfer with Those of This Study

XV. APPENDICES

TEMPERATURE MEASUREMENT

All temperatures were measured by one or more of the following instruments: mercury-in-glass thermometers, platinum-resistance thermometers or thermocouples. Mercury-in-glass thermometers were used for measurements where large errors in temperature would have a minor effect on the experimental results. These measurements consisted of the room temperature, mercury-manometer temperatures, resistance-bridge temperatures and barometer temperatures. Except in cases where the thermometer was previously mounted on the equipment, the resistance bridge for example, each mercury-in-glass thermometer was calibrated in a water bath at 20, 25 and 30°C to the nearest 0.01°C.

A. PLATINUM-RESISTANCE THERMOMETERS

All absolute temperature measurements were taken with a platinum-resistance thermometer (Chem. Eng. #23446). This thermometer was purchased from Leeds and Northrup and calibrated for this study. Calibration of the thermometer was based on the resistance versus temperature relationship of platinum as predicted by a modification of the Callendar equation [55]. This temperature versus resistance relationship was

$$t = ((R_t - R_o) / \alpha R_o) + \delta(t/100 - 1)(t/100)$$

where R_t and R_o are the resistances of the platinum resistor at t° and 0°C , respectively. The two constants, α and δ , are experimental parameters for a particular platinum wire. Calibration

consisted of determining the ice-point resistance, R_0 , plus the resistance at two additional temperatures. A second resistance thermometer which had been calibrated by the National Bureau of Standards (Chem. Eng. #20121) was used to establish absolute temperatures during the calibration. The same resistance bridge and oil bath used during the calibration of the platinum thermometer were used for all measurements of the experimental Joule-Thomson coefficient temperatures.

The procedure used to calibrate the platinum thermometer was as follows. First, the ice points of the NBS-calibrated and the new thermometer were measured. The thermometers were inserted into a large Dewar flask that had been filled with distilled water and crushed ice made from distilled water. The crushed ice extended to the bottom of the flask and was stirred before each resistance measurement. A series of resistance measurements was taken by each thermometer with a Rubicon resistance bridge (Chem. Eng. #22687). A plug board was used to switch from one thermometer to the other. The ice-point resistance of each thermometer was read to the nearest 0.00005 ohm. The ice-point of the new thermometer was determined to be 25.5535 ohms. The ice-point of the NBS-calibrated thermometer was measured to be 25.5304 ohms which was in agreement with the ice-point resistance of 25.530 ohms listed on its calibration card.

Next, both platinum-resistance thermometers were inserted into the constant-temperature oil bath. A third platinum-resistance thermometer (Chem. Eng. #1033) and a second resistance bridge (Chem. Eng. #20866), in conjunction with a thyatron modulator, were used to maintain the oil bath at the desired temperature during the resistance

measurements. After the bath temperature had been maintained at the desired temperature by the automatic feature of the thyatron modulator for about one hour, equivalent manual settings were used and the automatic feature was turned off. This was done to prevent fluctuations of temperature during the resistance measurements. When the oil bath was controlled by manual settings, a slight drift usually developed. This drift was checked and adjusted if necessary to be less than 0.0010-ohm per hour prior to any measurement. Then a plot of resistance versus time was made at 100 second intervals for both thermometers. Usually a series of four to five resistances was taken with one thermometer. Then the resistance bridge would be shifted to the other thermometer and another series of resistance measurements would be recorded. This procedure was continued until two series of resistances were taken with the first thermometer and one series was taken with the second. To obtain a resistance from each thermometer simultaneously, it was necessary to extrapolate the series of resistance measurements from one thermometer to a time corresponding to a resistance measurement of the other thermometer. To minimize the extrapolation, a common time very close to that of the switching from one thermometer to the second was used. This procedure was used for three nominal temperatures of 100, 160 and 280^oF. These temperatures correspond to those of the experimental measurements at each end of the measured range and at one intermediate value. Using the measured resistances from the NBS-calibrated thermometer, a temperature corresponding to each measured resistance of the new thermometer was obtained. In this manner R_t versus $t^{\circ}\text{F}$ was obtained for three temperatures. Since

there were only two unknown constants in the modified Callendar equation other than the ice point which was previously measured, only two of the three resistance measurements were needed for the calibration. The 100 and 280^oF resistance measurements were used. The third measurement at 160^oF was used as a check on the calibration and the agreement was within 0.0005^oF. Other pertinent values recorded during the calibration are given in Table 10.

At this point the relationship between temperature and resistance are included to aid in the understanding of the limitations of the measurements. A change in resistance of 0.0001-ohm is approximately equal to a temperature change of 0.002^oF. The resistance bridge was read directly to 0.0001-ohm and estimated to the nearest 0.00005-ohm. The reading error was therefore 0.000025-ohm, representing a temperature change of 0.0005^oF. This reading error is approximately one-half the value normally given. The increased sensitivity of the resistance measurements was due, in part, to the increased distance between the galvanometer and scale which measured the deflection. A two-meter distance was used instead of the standard one-meter distance. This added distance doubled the response of the galvanometer. The reduced light intensity required the galvanometer to be housed. All galvanometers used in this study were operated at a two-meter distance.

Even though the calibration of the two thermometers agreed with 0.0005^oF and the precision of the absolute temperature measurements of the NBS-calibrated thermometer was better than 0.002^oF, the accuracy of the new thermometer is claimed to only 0.05^oF in this study. This discrepancy is due to the calibration of the resistance bridge. The

manufacturer of the bridge did not furnish a calibration card for the changes in bridge-resistance readings due to changes in the bridge temperature. The resistance coils were made of manganin. In the range of room temperatures the resistance of manganin wire as a function of temperature can be represented by [56]

$$R_t = R_{25}(1 - a(t - 25^{\circ}\text{C}) - b(t - 25^{\circ}\text{C})^2) \quad .$$

The constants, a and b , in the above equation were determined from an average of the constants of five 10-ohm manganin coils with NBS calibrations. The values of the constants used for this study were

$$\begin{aligned} a &= 6 \times 10^{-7} \\ b &= 4 \times 10^{-6} \end{aligned}$$

The above resistance correction for bridge temperature changes was applied to all resistance measurements. The magnitude of this correction ranged from 0.0-ohm at 25°C to 0.0015-ohm at 32°C and 40 ohms total resistance. The above resistance curve compared favorably to an experimental curve determined for a similar resistance bridge. The advantage of using the above equation was in the writing of computer programs.

Besides the resistance-bridge calibration for temperature changes of the bridge, two other possible sources of error in the resistance measurements were constantly checked. These sources were the bridge zero adjustment and the bridge ratio adjustment. Bridge temperature also affected these adjustments but the typical error was usually less than 0.0002-ohm for a 3 to 4°C change in room temperature.

The platinum-resistance thermometer heating effect is a possible source of error but was considered negligible due to the large volume of oil in the bath. Therefore the claimed absolute temperature error of 0.05°F which represents a resistance error of approximately 0.0025-ohm is thought to be conservative.

B. THERMOCOUPLES

Two thermocouple networks were used in this study to measure the temperature change across the porous thimble. Each network consisted of three thermocouples wired in series. All thermocouples used copper-constantan junctions. (Actually "Advance" which is the Driver-Harris Company tradename for constantan was used.) A precise calibration of the thermocouple networks actually used in this study was not practical. The interior wires were only seven inches long and could not reach from the oil bath to an adjacent ice bath. Therefore a segment of wire was taken from each spool before and after the segment used for the thermocouple networks. Two other thermocouples, labeled A and B, were made from these additional segments. The interior wires of A and B were fourteen inches long. This additional length permitted the constant-temperature oil bath and platinum resistance thermometer of the research apparatus to be used in the calibration. Using the resistance thermometer to establish the temperatures, thermocouples A and B were calibrated over the experimental range. Results of this calibration are listed in Table 9. The experimental points were fitted to an equation of the form

$$\mu V = at + bt^2 + ct^3$$

where V is in microvolts and t in $^{\circ}\text{C}$. Caltech Computing Center's least-squares program was used to determine the constants a , b , and c . The above equation was recommended by NBS [57] for thermocouple calibrations. Both the A and B thermocouples had essentially the same standard deviation to the curve-fitted equation. Therefore it was assumed that the thermocouple networks used in this study had similar calibrations. The results listed in Table 9 are for one thermocouple and must be multiplied by three to correspond to the networks used in this study. The largest difference between the least-squares curve and any experimental point was 0.48 microvolts in 4504.4 total microvolts or 0.012%. This difference was considered negligible, especially since the temperature change was calculated from the slope of the calibration curve.

One Wenner potentiometer (Chem. Eng. #20805) was used for all thermocouple readings. This potentiometer could be read directly to 0.1 microvolt and estimated to the nearest 0.05 microvolt. Since the same potentiometer used in the calibration curve was also used for the experimental measurements, any error resulting from the standard cell would be reduced. The standard cell was checked by "bucking" it against the standard cells of other potentiometers in the Laboratory. This procedure indicated the standard cell to be in excellent agreement with its calibration certificate. Laboratory records indicated the other standard cells to be in agreement with their certificates.

The largest unknown value in the thermocouple measurements was from parasitic EMF. No direct measurement of this EMF was obtained since the thermocouple networks could not be easily grounded. Estimates

were made by the following method. With no gas flowing through the calorimeter, thermocouple readings were taken of the temperature change across the porous thimble at the four isotherm temperatures. A zero reading should have been measured at each temperature. Non-zero readings were attributed to parasitic EMF. In this manner the maximum parasitic EMF was determined to be less than 0.2 microvolt.

Error in the measurement of the temperature change used in the calculation of the Joule-Thomson coefficient induced an error in the absolute temperature of the coefficient, and vice versa. For instance, thermocouple readings from which the temperature changes were calculated had errors of up to 0.20 microvolt due to parasitic EMF, 0.05 microvolt due to inaccuracies in reading the potentiometer, and 0.05 microvolt due to the thermocouple calibration for a total of 0.30 microvolt. This 0.30 microvolt would correspond to a maximum error of 0.0042°F in the temperature change. An error of 0.0042°F in the temperature change would induce an additional error of 0.0021°F in the gas temperature. This 0.0021°F , when combined with the previously estimated error of 0.05°F in the temperature due to resistance thermometer inaccuracies, would result in a possible error of 0.052°F . Since the temperature of the gas was used to enter the thermocouple calibration curve, it would likewise induce an error in the measured temperature change. An error of 0.052°F in the gas temperature would cause a maximum error of only $5 \times 10^{-6} \text{ }^{\circ}\text{F}$ per microvolt in the temperature change. Since the largest thermocouple reading was less than 130 microvolts, this latter error was neglected.

APPENDIX II

PRESSURE MEASUREMENTS

All pressure measurements were made with one or more of the following instruments: mercury barometer, mercury manometer, pressure-balance system [40,58] and high-pressure manometer [59].

Atmospheric pressure was measured with a brass-tube mercury barometer. Corrections to the barometric pressure were made for temperature [60], gravity in Pasadena, and elevation differences between the barometer and apparatus. Pressure measurements were recorded to the nearest 0.01 mm Hg. The accuracy of the atmospheric pressure was estimated to be ± 0.1 mm Hg because of reading and adjustment errors.

The pressure of the gas, prior to being throttled, was measured either by a mercury manometer which had one leg open to the atmosphere or by the pressure-balance system. Both instruments relied on the barometric pressure for absolute values of the pressure. The mercury manometer was read by a cathetometer to the nearest 0.01 mm Hg. Because of mercury curvature and cathetometer inaccuracies, the accuracy of the mercury manometer readings was estimated to be ± 0.05 mm Hg. The pressure-balance system was used when the pressure exceeded two atmospheres gauge. Pressures from the pressure-balance system were read to the nearest 0.05 psi. Due to changes in the density of the oil line between the mercury trap and balance, the pressure measurements were estimated to have an accuracy of 0.1 psi. Therefore the maximum error in the absolute pressure would be approximately 0.1 psi.

The pressure change across the porous thimble was measured with a differential mercury manometer and/or the high-pressure manometer. The differential-mercury manometer was used for all pressure-change measurements even though the high-pressure manometer was connected and working. The primary advantages of the mercury manometer were its higher accuracy (0.05 mm Hg to 0.3 mm Hg), speed in obtaining a pressure, and constant visual indication. Its maximum working pressure was 100 psi. All measurements of the pressure change were corrected for temperature, gas densities in the manometer and Pasadena gravity.

The error in the absolute pressure induced by error in the pressure change was small and therefore neglected.

P R O P O S I T I O N S

PROPOSITION I

The method of oxidation-reduction cycling as used in the preparation of metal powders by Czanderna [1] is proposed for the removal of oxidation products and undesirable discoloration from the surfaces of rare coins. An easily constructed reactor is described in which to carry out the reactions.

INTRODUCTION

The present-day art of rare coin cleaning leaves much to be desired. Commercial and homemade cleaners consist primarily of liquid acids or abrasive pastes which remove a fraction of the metal surface during the cleaning process. A uniformly-cleaned surface with these cleaners is difficult to obtain without the removal of an excessive amount of metal due to crevices in the design and also lettering on a coin. Coins cleaned in liquid acids have a tendency to corrode or change to an abnormal color, e.g., grey copper.

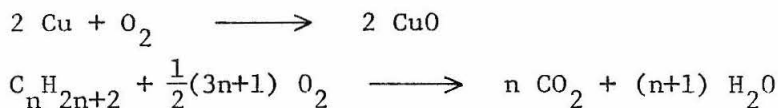
The removal of metal from the surface of a coin, either by wear or chemical action, reduces its value significantly. For example, an uncirculated coin of a particular date is generally 25 to 50 percent more valuable than an almost uncirculated coin. An old coin with an attractive appearance is treasured by collectors and sold at premium prices by coin dealers. Since copper coins have the greatest tendency to chemically change to an undesirable color, the oxidation-reduction cycling method was tested with copper coins. The method is applicable for all metallic coins even though not specifically tested.

The proposed oxidation-reduction cycling method offers a method of cleaning discolored coins without chemical or mechanical damage. The method is more difficult and less economical than liquid cleaning if coin damage is not considered. Commercial cleaners range in cost from about \$2.50 for one-step cleaners to \$30.00 for a multi-step cleaning process consisting of six to eight different liquids. There are many coins valued above \$2000 [2] and some have been sold at auctions at prices up to \$47,000. The slightly higher cost of the oxidation-reduction process is not of great concern provided the method enhances rather than decreases the value of the coins.

THEORY

The proposed oxidation-reduction cycling method consists of repeated exposure of the coins to pure oxygen at a constant elevated temperature, followed by chemical reduction with hydrogen at approximately the same temperature. Typical reactions which might occur during the oxidation and reduction steps are:

Oxidation



Reduction



The removal of undesirable surface colors without the removal of metal is the primary benefit of the oxidation-reduction cycling process.

The possibility of a spontaneous reaction between hydrogen and oxygen was considered. If hydrogen comes into contact with oxygen only at room temperature and atmospheric pressure and the reactor temperature is kept below 500°C, the possibility of a spontaneous reaction is negligible. A good reference on the hydrogen-oxygen reaction is given by Pease [3].

EQUIPMENT

The oxidation-reduction cycling reactions were carried out in the apparatus illustrated in Figure 1. The reactor consists of a 4-foot length of Pyrex tubing with an inside-diameter of 9 mm. A 400-watt tape heater, coiled around the exterior of the Pyrex tube, supplied the energy to increase the reaction rates. Temperature of the reactor was manually controlled by a Variac. Glass wool surrounded the heater to prevent excessive heat losses to the environment. Rubber stoppers were used to seal the ends of the reactor. Hydrogen and oxygen entered and exited the reactor by 1/4-inch copper tubing which was inserted through a hole in each stopper. A mercury thermometer with a range of -10 to 400°C was placed inside the reactor to measure the reaction temperature. Glass wool, wrapped around the thermometer, prevented direct contact between the thermometer and walls of the reactor.

Large thermal gradients occurred in the axial direction in the reactor because the temperature of the inlet gas was increased as it flowed through the heated section. The oxidation-reduction reaction was carried out at the hottest location in the reactor which was at the downstream end of the tape heater. The bulb of the mercury thermometer was located in the hottest section. Even when the reactor was operated at a temperature of 450°C, the ends of the reactor remained near room temperature due to the small heat capacity of the gases.

After passing through the reactor, the exhaust gas was bubbled through a beaker filled with water. The bubbling process prevented

air from leaking into the reactor and helped indicate the flow rate of the oxidizing or reducing gas. The reactor was located in the hood for the purpose of disposing the exhausted hydrogen or oxygen. Safety plate glass on the front of the hood provided protection in the event of an explosive reaction between hydrogen and oxygen.

High-pressure storage cylinders served as a source of the reactant gases. Gas pressure was reduced to 10 psig at the cylinder regulator. A flame arrester and throttle valve after the regulator further reduced the pressure so that the gas pressure in the reactor was approximately 3 inches of water above atmospheric. A rotameter in the inlet gas line was used to measure the flow rate.

CLEANING PROCEDURE

Prior to placing the coins into the reactor, all foreign material not chemically attached to the surface was removed in an ultrasonic cleaner using soapy water. The coins were then rinsed in distilled water and air dried. Then they were placed on glass wool and inserted into the reactor. Room temperature oxygen from the storage cylinder initially flowed through the reactor at a rate of 20 ft³/hr to flush the air. After a two-minute flushing period, the oxygen flow was reduced to 1 ft³/hr and the Variac controlling the heater was set for a reactor temperature of 300°C in the reaction zone. The initial oxidation cycle lasted 30 minutes at 300°C and each subsequent oxidation cycle was increased by an additional thirty minutes until the coins were clean. Each oxidation cycle was followed by a hydrogen reduction cycle. The total number of oxidation and reduction cycles depended on the original condition of the coin. Three to four complete cycles were typical.

Following the oxidation cycle, the heater was turned off with oxygen continuing to flow through the reactor. When the reactor temperature cooled to below 60°C, the oxygen flow was stopped and the oxygen cylinder replaced with a hydrogen cylinder. Similarly, room temperature hydrogen initially flowed through the reactor at 20 ft³/hr to flush the remaining oxygen from the reactor. Then the heater Variac was set for a reactor temperature of 325°C. The duration of each reduction cycle was approximately the same length of time as the preceding oxidation cycle. Observation of the coin through the glass reactor made possible the shortening of the reduction cycle at times. After the reduction cycle,

the heater was turned off while hydrogen continued to flow in the same manner as the oxidation cycle. Upon cooling to below 50°C, the coins were removed from the reactor and inspected with a microscope. The condition of the coins determined if further oxidation-reduction cycling was needed.

RESULTS AND CONCLUSIONS

Photographs illustrating the results of liquid cleaning and the oxidation-reduction cycling method are given in Figures 2a through 2d. All photographs were taken with 48-power magnification and show only a small portion of the flat surface of various copper pennies. Figure 2a shows the typical surface of a newly-minted penny. Figure 2b illustrates the removal of metal by liquid cleaners when used according to the instructions. The top half of this penny was protected from the cleaner with grease during cleaning. Figure 2c indicates what can happen to the surface of a coin when one tries to do a thorough job around the lettering. The surface was highly etched. Figure 2d illustrates the surface of a penny after having undergone three complete oxidation-reduction cycles. The penny was initially oxidized to the typical brown color through normal circulation. The lines in the photograph are from scratches due to circulation rather than the cleaning process.

The oxidation of copper coins and subsequent reduction with hot hydrogen proved to be a successful method of removing oxidation products from the surface without damage to the coins. The oxidation-reduction process is more uniform than most liquid cleaners as gases penetrate the crevices in the design better than liquids. Unlike liquid cleaners which remove a small amount of metal each time, the cycling process can be used repeatedly without damage to the coin. The proposed process is slower but several coins can be cleaned simultaneously. Disadvantages include the obtaining and setting up of the apparatus and the strict adherence to safety precautions when mixing

hydrogen and oxygen. A larger reactor would be necessary for coins having a diameter larger than 9 mm.

Long range effects of the oxidation-reduction process were not observed. Prior to cleaning any valuable coins, the tendency for cleaned coins to corrode or reoxidize to an undesirable color should be observed.

Coins can be ruined if the reactions take place at too high a temperature. To prevent distortion of the coins, do not heat them above the recrystallization temperature, which for pure metals is approximately 40% of the absolute melting temperature [4]. The recrystallization temperature for copper is approximately 370°C [5]. One experimental cleaning cycle at 450°C resulted in poorly cleaned coins with severely etched surfaces. An extremely thin layer of copper peeled off three different pennies. A silver dime also in the reactor became copper colored. The metallic ions apparently became highly mobile at the higher temperature.

Another point to consider before cleaning coins by any method is the desired final color. Coins cleaned with the oxidation-reduction method had a slight reddish-orange color rather than the yellowish-orange color of newly minted coins. Upon exposure to the atmosphere for several days, a slow change to the mint color was noticeable. Whether coins over 100 years old should have the color of newly minted ones is a matter of personal choice.

If the coin initially had an undesirable color, the oxidation-reduction method would certainly improve its appearance.

REFERENCES

1. A. W. Czanderna, "Magnetic Susceptibility Changes in Silver Powders During Oxidation-Reduction Cycling," J. Phys. Chem. 71, 1967, pp. 770-771.
2. R. S. Yeoman, A Guide Book of United States Coins, 22nd Ed., Western Publishing Co., Racine, Wisconsin, 1966.
3. R. N. Pease, B. Lewis and H. S. Taylor, Combustion Processes, Princeton University Press, Princeton, 1956, pp. 160-174.
4. D. S. Clark and W. R. Varney, Physical Metallurgy for Engineers, 2nd Ed., D. Van Nostrand Co., New York, 1966, p. 358.
5. W. A. Lange, Handbook of Chemistry, 10th Ed., McGraw-Hill, New York, 1961, pp. 246-247.

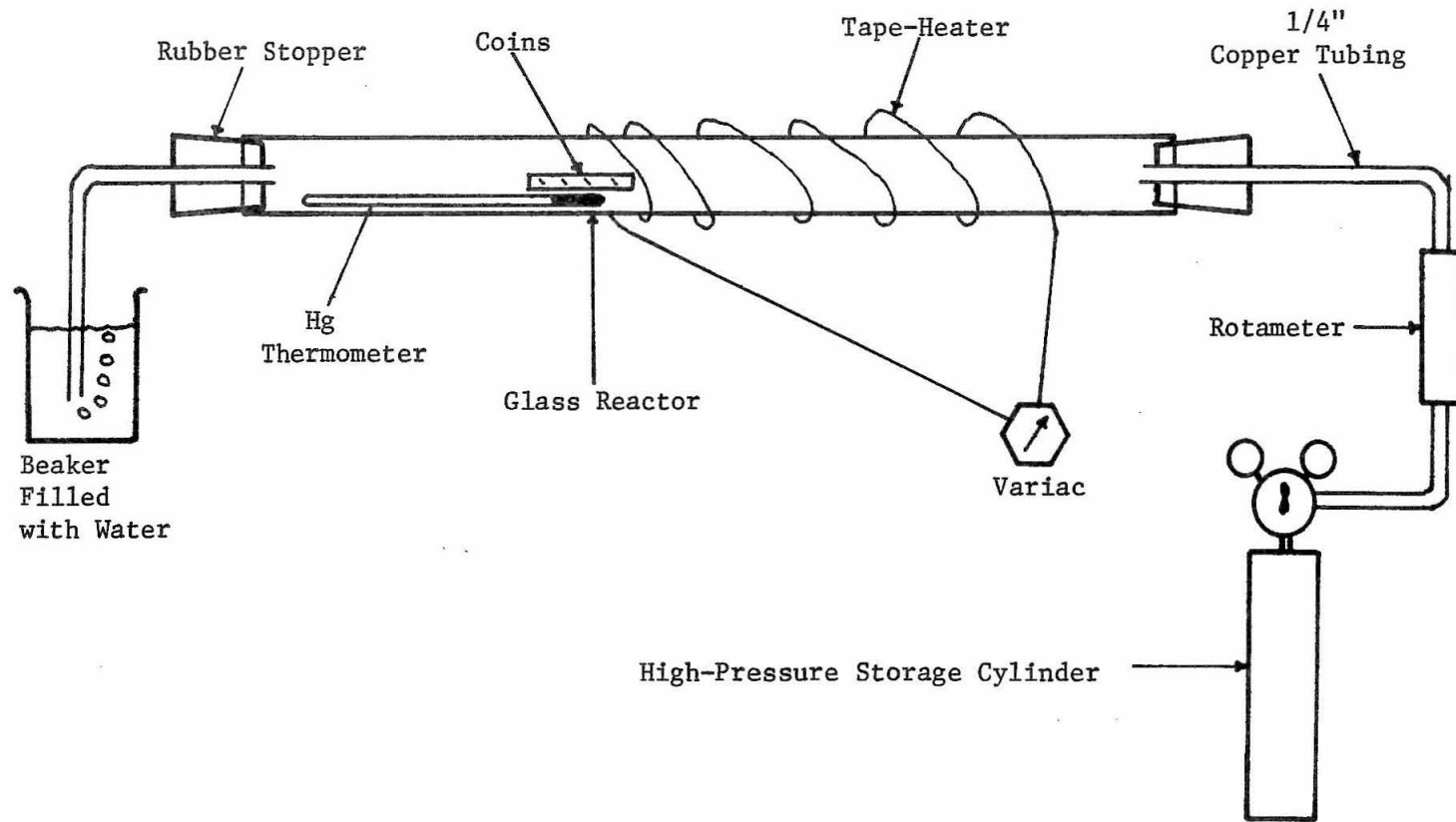


Fig. 1. Drawing of Reactor

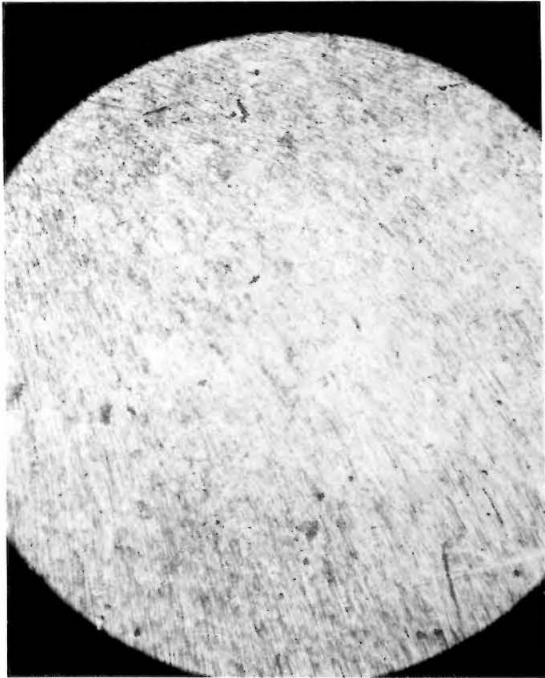


Fig. 2a. Typical surface of new coin.

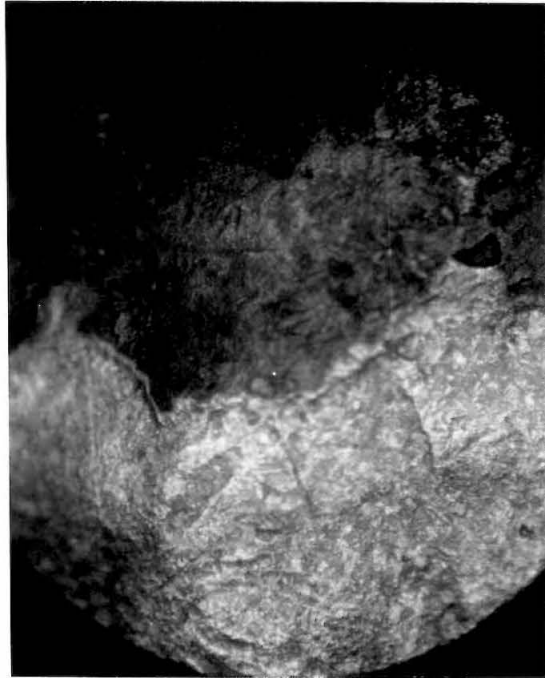


Fig. 2b. Surface of coin cleaned with liquid cleaner according to directions.

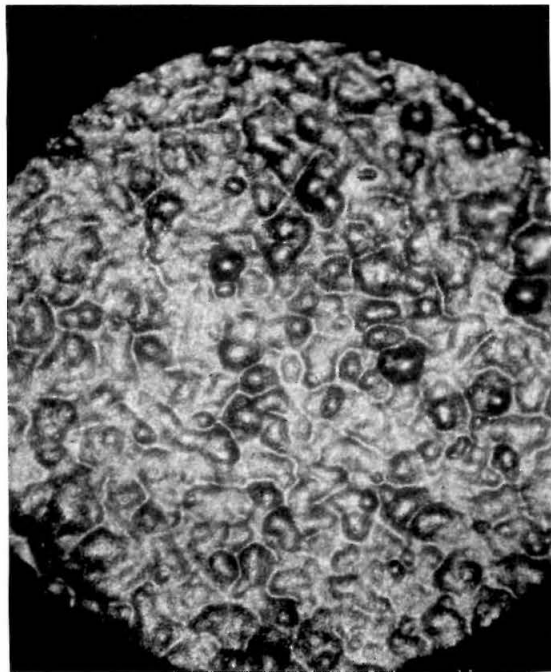


Fig. 2c. Surface of coin cleaned in a liquid cleaner with thorough job around lettering.

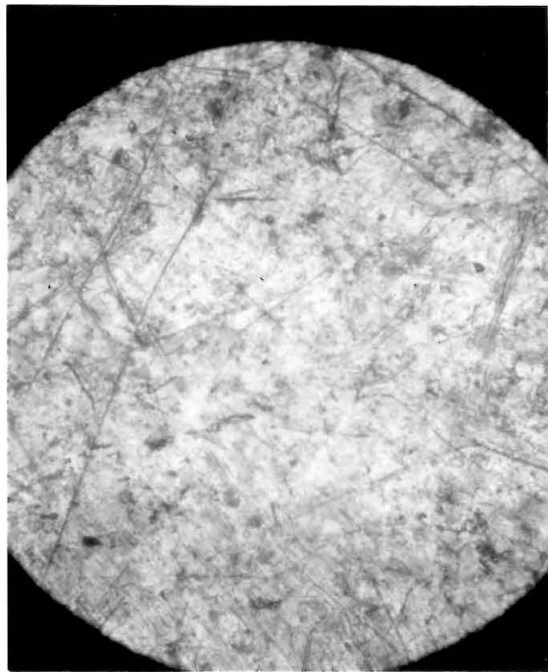


Fig. 2d. Surface of coin cleaned by oxidation-reduction method.

PROPOSITION II

The galvanic response of a Hersch detector [1] is related to the concentration of oxygen of a gas sample passing through it. By varying the load-resistance of the cell, concentrations of oxygen from 0 to 50,000 ppm may be correlated with the output of a one-millivolt recorder. An equation is proposed which relates the load-resistance of the detector to the response of a millivolt recorder for a given concentration of oxygen.

INTRODUCTION

A Hersch cell is a specific and sensitive detector of oxygen which offers higher sensitivities than possible with other types of oxygen detectors. It consists of a silver cathode and lead anode in contact with an electrolyte containing hydroxide ions. A carrier gas continuously flows through the cell. Oxygen in the carrier gas is reduced at the cathode and an electric current is generated according to the following electrode reactions:

Cathode



Anode



Hersch cells are normally operated either with continuous flow through the cell of the gas to be analyzed, or with a "blank" carrier gas and the oxygen-containing gas injected in pulses. For

cells operated in the continuous manner, mathematical equations relating current output to concentration of oxygen have been proposed [1, 2]. Since oxygen constantly flows through the cell, an ammeter can be used to measure the current output.

When the Hersch cell is operated in the pulse manner; small samples containing oxygen are injected into the carrier gas, similar to the injection method of gas chromatography. Current output of the cell varies according to the concentration of oxygen within the cell. Therefore the use of an ammeter is not feasible to measure the current output, since it would be difficult to record the maximum or average current. To measure the current a load-resistor is placed in the circuit of the Hersch detector and a millivolt recorder is used to measure the voltage drop across the resistor. In this manner, a permanent record of the output of the cell can be obtained.

Concentrations of oxygen up to 50,000 ppm can be analyzed when small samples are injected into the carrier gas. Since millivolt recorders are somewhat limited in range, different resistors are used to keep the voltage drop within the limits of the recorder. The value of the resistor which is placed in the circuit of the Hersch cell affects the current output of the cell. The effects of a resistor are determined by calibrating the cell using pulses of known concentrations of oxygen. If several different resistors are used in the analysis of widely-varying concentrations of oxygen, the present method of operation is to individually calibrate each resistor [3,4]. Since cell life is difficult to determine except by actual service [5], the calibrations

are normally repeated daily and sometimes more often for very accurate studies. The proposed equation relating the output of a Hersch detector to load-resistance for a given concentration of oxygen will reduce the amount of calibration data required to that for a single resistor.

THEORY

The purpose of this section is to relate the effects of the load resistance to the electrical output of a Hersch detector for a given concentration of oxygen. It was assumed that the Hersch cell could be represented by a current source. The internal resistance of the current source is in parallel to the load resistor. Hersch [1] implied a similar circuit for the continuous-flow detector. In addition, it was postulated that the cell current is proportional to the partial pressure of the oxygen at the cathode. This relationship can be stated mathematically:

$$i = k \bar{P}_{O_2} \quad (1)$$

where \bar{P}_{O_2} is the partial pressure of the oxygen and k is the constant of proportionality. For a particular cell operated at a specified flow rate of the carrier gas, the partial pressure of the oxygen is proportional to the concentration of oxygen in the injected sample:

$$\bar{P}_{O_2} = k_1 C_{O_2} \quad (2)$$

where C_{O_2} is the concentration of oxygen. Combining Equations (1) and (2) yields

$$i = k_2 C_{O_2} \quad (3)$$

where $k_2 = k k_1$. The current produced by the cell is equal to the voltage of the cell divided by the total resistance of the cell and external circuit. Therefore Equation (3) can be restated:

$$E/R_{tot} = k_2 C_{O_2} \quad (4)$$

where E is the cell voltage and R_{tot} the total resistance of the cell. The total resistance is related to the internal resistance and load resistor by:

$$1/R_{tot} = (1/R + 1/\rho) = (1 + R/\rho) / R \quad (5)$$

where R is the load resistor and ρ the internal resistance of the cell. Combining Equations (4) and (5) yields

$$E = k_2 C_{O_2} R / (1 + R/\rho) \quad (6)$$

The peak height, H , of the millivolt recorder is a linear function of the cell voltage and this relationship can be expressed:

$$H = k_3 E \quad (7)$$

Combining Equations (6) and (7), the proposed equation relating the response of a millivolt recorder to load-resistance for a given oxygen concentration is obtained:

$$H = k_4 C_{O_2} R / (1 + R/\rho) \quad (8)$$

where $k_4 = k_2 k_3$. The constant, k_4 , is not a true constant, since it is a function of the flow rate of the carrier gas, Hersch cell design, and cell efficiency. For a given cell and flow rate, it does remain constant provided the efficiency of the cell does not change. The value of k_4 is obtained by calibrating the cell with oxygen samples of known concentration. Even when the day-to-day efficiencies of the cell vary, new values of k_4 can be obtained by recalibrating the cell frequently.

The values of k_4 and ρ were obtained by simultaneously solving Equation (8) using the data of the 1 and 1000-ohm resistors listed in Table 1. In particular, values of the slopes of the peak height versus oxygen concentration for the 1 and 1000-ohm resistors were 7.03×10^{-5} and 3.04×10^{-2} mv/ppm, respectively. Using these data, the values of k_4 and ρ were determined to be 7.04×10^{-5} mv/ohm-ppm and 760 ohms, respectively. Inserting these values into Equation (8) yields

$$H = 7.04 \times 10^{-5} C_{O_2} R / (1 + R/760) \quad . \quad (9)$$

Equation (9) is applicable only for the particular cell used to obtain the data listed in Table 1. Since the data of only two of the seven resistors were used to obtain Equation (9), a good correlation with the remaining five resistors would substantially support the proposed equation.

EXPERIMENT

The data listed in Table 1 were experimentally determined by Blakemore [6]. A Hersch cell similar to the design of Phillips [4] was used in the measurements. The relationship between oxygen concentration and recorder output was determined for seven different resistors: 1, 3, 10, 30, 100, 300 and 1000 ohms. Eight primary gas mixtures, ranging from 20 to 37,390 ppm of oxygen in argon, were used for the calibration. Each of the eight primary samples were further diluted with argon to yield a larger variation in the concentration of oxygen. Sample volumes of 0.2 cc were injected into the argon carrier gas which flowed through the cell at the rate of 20 cc/min. Ninety-five percent of the data were estimated to have an error of less than 5%.

RESULTS AND CONCLUSIONS

The proposed equation which relates the load resistance of a Hersch detector to the response of a millivolt recorder for a given concentration of oxygen is

$$H = k_4 C_{O_2} R / (1 + R/\rho) \quad (8)$$

where the constant, k_4 , and internal cell resistance, ρ , are functions of a particular Hersch cell. For the cell and operating conditions used to determine the data listed in Table 1, values of k_4 and ρ were calculated to be 7.04×10^{-5} mv/ohm-ppm and 760 ohms, respectively. Inserting these values into Equation (8) yields

$$H = 7.04 \times 10^{-5} C_{O_2} R / (1 + R/760) \quad (9)$$

Equation (9) was used to calculate the peak height of the millivolt recorder as a function of the concentration of oxygen for the seven different resistors listed in Table 1. The results of these calculations are represented by the solid lines in Figures 1 and 2. The experimental data listed in Table 1 were also plotted in these figures in order to compare the results.

The agreement between the calculated values and the experimental values is well within the experimental error of the data. The poorest agreement resulted from the data of the 3-ohm resistor. The direction of the disagreement could be explained by a loss in cell efficiency. Since the data of each resistor does agree with the calculated values, the proposed equation would reduce the amount of

calibration data required for this particular cell. The more general expression, Equation (8), should apply to all cells of similar construction.

REFERENCES

1. P. A. Hersch, "Trace Monitoring in Gases Using Galvanic Systems," Analytical Chemistry 32, 1960, pp. 1030-1040.
2. Advances in Analytical Chemistry and Instrumentation III, Wiley, New York, 1964, p. 219.
3. G. E. Hillman and J. Lightwood, "Determination of Small Amounts of Oxygen Using a Hersch Cell as a Gas Chromatography Detector," Analytical Chemistry 38, 1966, pp. 1430-1433.
4. T. R. Phillips, E. G. Johnson, and H. Woodward, "The Use of a Hersch Cell as a Detector in Gas Chromatography," Analytical Chemistry 36, 1964, pp. 450-452.
5. W. J. Baker, J. F. Combs, T. L. Zinn, A. W. Wotring and R. F. Wall, "The Galvanic Cell Oxygen Analyzer," Industrial and Engineering Chemistry 51, 1959, pp. 727-730.
6. J. E. Blakemore, personal communications, 1970.

NOTATION

cc	cubic centimeters
C_{O_2}	concentration of oxygen in ppm
E	voltage of cell
H	peak height of millivolt recorder in millivolts
i	current of cell
k, k_1 , etc.	constants of proportionality
mv	millivolts
\bar{P}_{O_2}	partial pressure of oxygen
ppm	parts per million by volume
R	load-resistor in ohms
R_{tot}	total resistance of cell
ρ	internal resistance of cell

TABLE 1

EXPERIMENTAL HERSCH-CELL DATA

Resistance (Ohms)	Oxygen Concentration (ppm)	Peak Height (mv)
1000	180	5.04
1000	138	4.26
1000	137.5	4.37
1000	140.5	4.35
1000	74.7	2.55
1000	73.7	2.39
300	20	.311
100	117.3	.725
100	47.2	.319
100	135.5	.794
30	180	.386
30	117.3	.254
30	326	.656
30	398	.717
30	172	.356
30	180	.375
30	135.5	.274

TABLE 1 - Continued

Resistance (Ohms)	Oxygen Concentration (ppm)	Peak Height (mv)
10	770	.556
10	540	.377
10	326	.229
10	940	.653
10	600	.412
10	398	.247
10	1200	.824
3	3890	.782
3	3080	.626
3	2520	.510
3	2010	.404
3	1200	.240
1	8260	.580
1	5620	.395
1	3140	.218

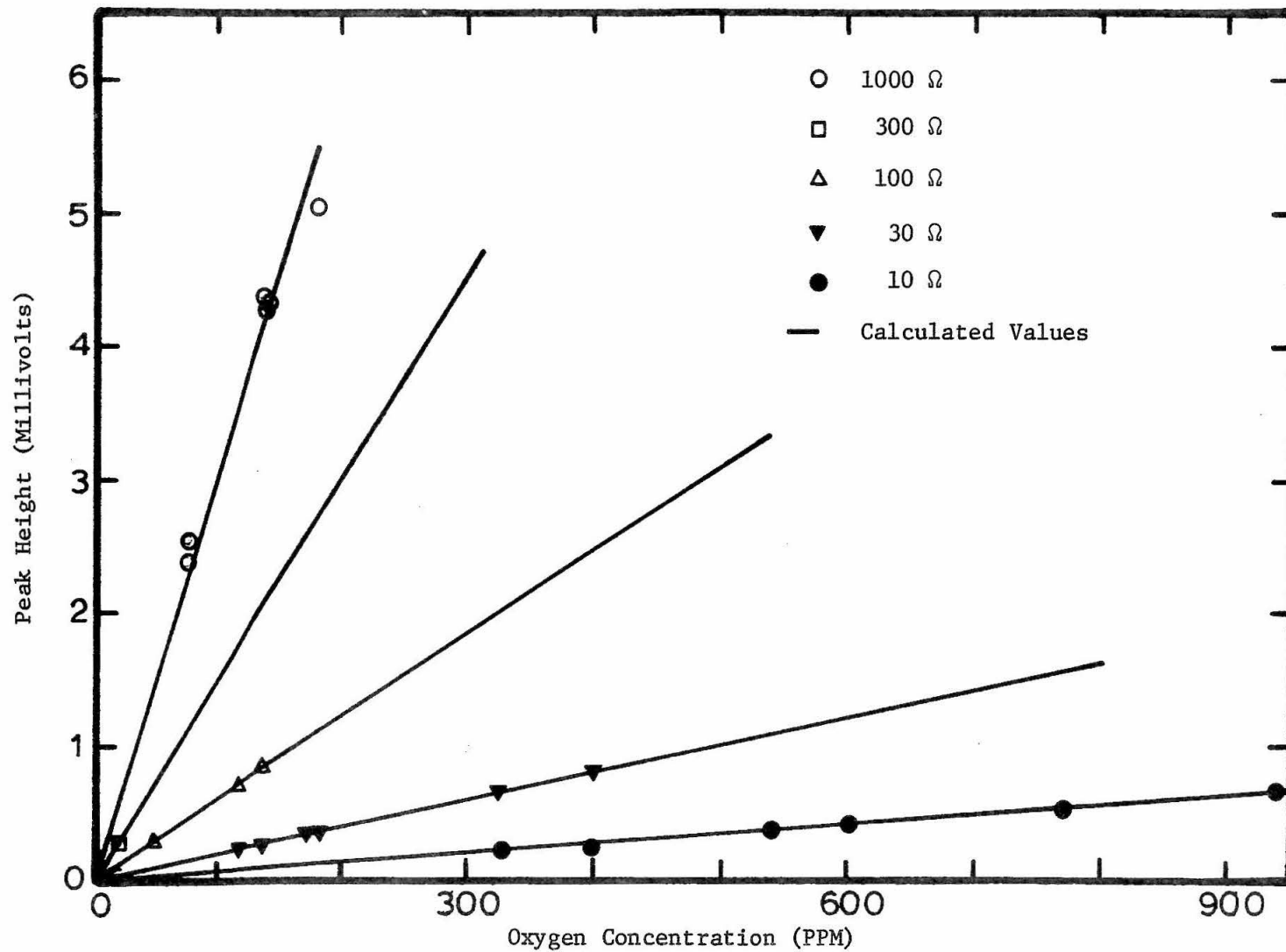


Fig. 1. Oxygen Concentration vs Peak-Height for Five Different Resistors

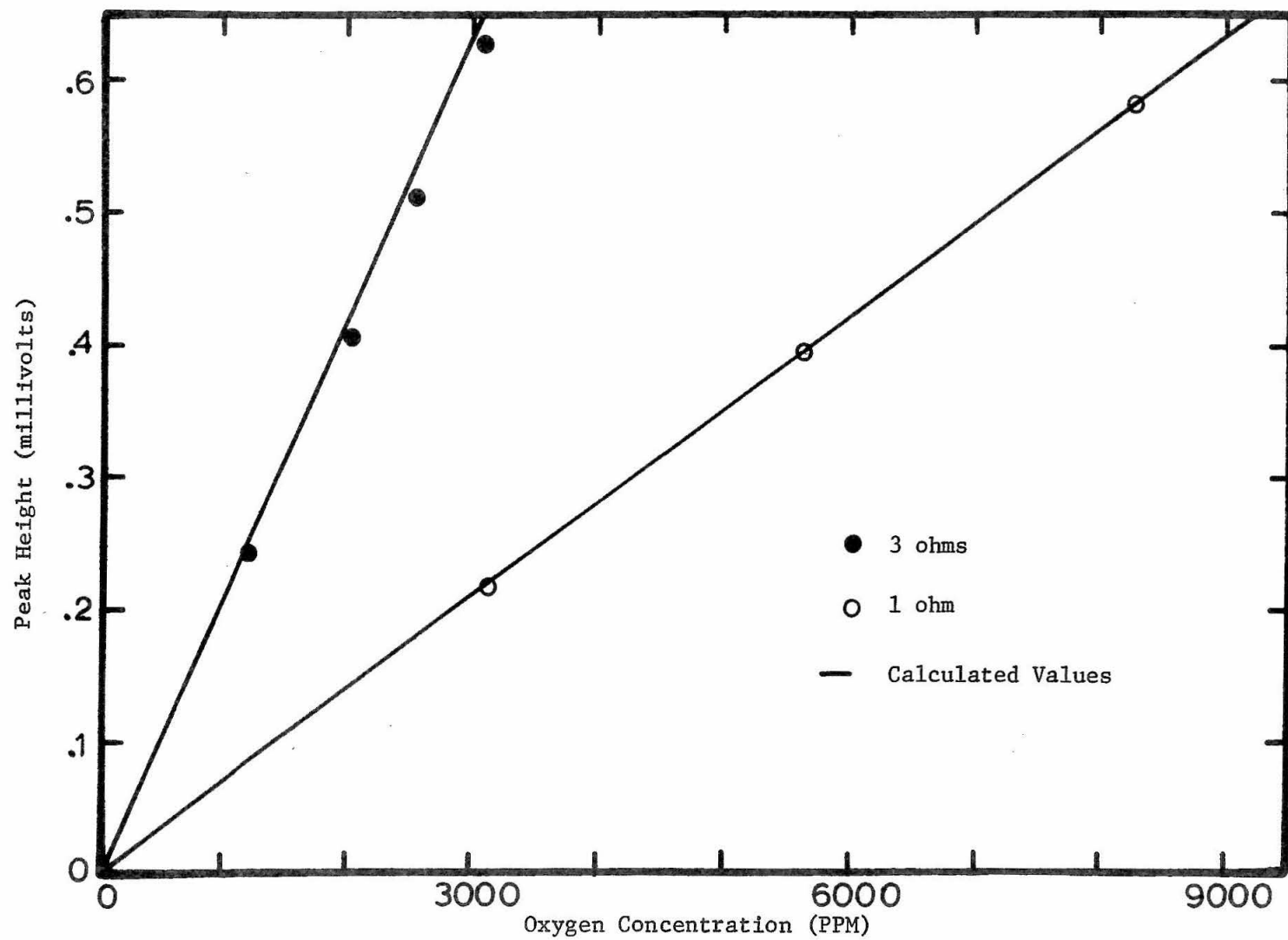


Fig. 2. Oxygen Concentration vs Peak-Height for Two Resistors

PROPOSITION III

A design for a rotameter which can be used as a viscometer is proposed. Design features significantly increase the normally undesirable viscosity dependence of a standard rotameter. Mathematical equations describe the viscosity relative to the position of the float.

INTRODUCTION

Since the 1940's rotameters have become increasingly important in the measurement of flow rates of fluids. Design work has been primarily in the area of reducing the dependence of the flow rate on fluid properties [1,2,3]. In this study a rotameter has been designed to take advantage of the viscosity dependence in order that it might be used as a viscometer. Advantages of the proposed viscometer are its ability to monitor the viscosity of continuous-flow processes while maintaining simplicity in design.

DISCUSSION

The proposed viscometer design is illustrated in Figure 1.

Features which separate the proposed viscometer from typical rotameters are: (1) a streamlined float which has its wall parallel to the tapered glass tube, and (2) a small-diameter rod which maintains the float concentric with the glass tube.

The equation relating the position of the float to the viscosity of the fluid was derived by making a steady-state, force balance on the float. The force balance yields:

$$P'_2 A'_2 - P'_1 A'_1 - \int_{A'_s} P'_s \sin \theta dA'_s = - \tau_{rz} \Big|_{\text{float}}^{A''_s} - V_f \rho_f g_x \quad (1)$$

pressure
drag
gravity

where:

- A'_2 is the cross sectional area of the top of the float
- A'_1 is the cross sectional area of the bottom of the float
- P'_2 is the pressure applied to A'_2
- P'_1 is the pressure applied to A'_1
- P'_s is the pressure applied to A'_s
- A'_s is the surface area of the sides of the float
- A''_s is the surface area of the entire float
- z is the coordinate-direction parallel to the taper of the float
- x is the coordinate in the vertical direction
- τ_{rz} is the momentum flux

- V_f is the volume of the float
 ρ_f is the density of the float
 g_x is the component of gravity in the x direction
 θ is the angle between the x and z coordinate directions

An exact solution to the above equation would be difficult. If the taper of the glass tube is limited to a small angle, Equation (1) can be simplified by assuming that the wall of the tube and the float form coaxial, right-circular cylinders at each float position (See Figure 2). Equation (1) then becomes:

$$A_{12}(P'_2 - P'_1) = -A_s \tau_{rx} \Big|_{r=kR} - V_f \rho_f g_x \quad (2)$$

where kR is the arithmetic average of the top and bottom radii of the float, A_{12} the cross-sectional area of the float using radius kR , A_s the surface area on the sides of the float, and R the inside radius of the tube.

Equations describing the steady, laminar, Newtonian flow of an incompressible fluid in the annulus of the above geometry have been derived [4] and the results are:

(i) The average velocity

$$\langle V_x \rangle = \frac{(P_1 - P_2)R^2}{8\eta L_f} \left(\frac{1 - k^4}{1 - k^2} - \frac{1 - k^2}{\ln(1/k)} \right) \quad (3)$$

(ii) The volume rate of flow

$$Q = \frac{\pi(P_1 - P_2)R^4}{8\eta L_f} \left((1 - k^4) - \frac{(1 - k^2)^2}{2 \ln(1/k)} \right) \quad (4)$$

(iii) The momentum flux

$$\tau_{rx} = \frac{(P_1 - P_2)R}{2L_f} \left(\frac{r}{R} - \left[\frac{1 - k^2}{2 \ln(1/k)} \right] \cdot \frac{R}{r} \right) \quad (5)$$

where:

P is defined as $P + \rho g_x$

L_f is the length of the float

η is the viscosity of the fluid

R is the inside radius of the outer, coaxial cylinder.

Substituting Equations (3), (4) and (5) into Equation (2) yields:

$$A_{12}(P'_2 - P'_1) = \frac{-8\eta L_f Q \left[k^2 - \frac{(1 - k^2)}{2 \ln(1/k)} \right]}{R^2 \left[(1 - k^4) - \frac{(1 - k^2)^2}{\ln(1/k)} \right]} - V_f \rho_f g_x \quad (6)$$

A solution to Equation (6) is difficult to obtain since P'_1 and P'_2 are affected by the acceleration and deceleration of the fluid at the ends of the float. To obtain values for P'_1 and P'_2 , it was assumed that the pressures acting on each end of the float are equal to the corresponding pressures at each end of the annulus. This assumption is crude but the errors which are introduced will be similar at each float position. Calibrating the viscometer with a

fluid of known viscosity and determining all other viscosities relative to the calibration will decrease the error.

If the pressures at each end of the annulus, as determined by Equation (4), are used to replace P'_1 and P'_2 in Equation (6); the following result is obtained

$$\frac{8\eta QL_f}{R^2 [(1 - k^4) - \frac{(1 - k^2)^2}{\ln(1/k)}]} \left(\frac{A_{12}}{\pi R^2} - k^2 + \frac{1 - k^2}{2 \ln(1/k)} \right) = V_f \rho_f g_x - A_{12} \rho g L_f \quad (7)$$

Since V_f is equal to the product of A_{12} and L_f , and since R_f is equal to kR , the above may be rearranged to yield:

$$\frac{\eta \left[\frac{1 - k^2}{2 \ln(1/k)} \right] k^2}{(1 - k^4) - \frac{(1 - k^2)^2}{\ln(1/k)}} = \frac{\pi R_f^4 (\rho_f - \rho) g_x}{8Q} \quad (8)$$

The left-hand side of Equation (8) excluding the viscosity, η , is solely a function of the float position for a given viscometer, since

$$k = R_f / (R_f + x \tan \theta)$$

where R_f is the radius of the float and x the distance above the point where the radius of the float and glass tube are equal. Equation (8) can be expressed:

$$\eta F(x) = \frac{\pi R_f^4 (\rho_f - \rho) g_x}{8Q} \quad (9)$$

where

$$F(x) = \frac{k^2 \frac{(1 - k^2)}{2 \ln(1/k)}}{[(1 - k^4) - \frac{(1 - k^2)^2}{\ln(1/k)}]}$$

For a given viscometer, it is possible to calculate the viscosity from the position of the float using Equation (9), provided the flow rate and density of the fluid are known. The accuracy of the calculated viscosities would depend on the validity of the assumptions used to derive Equation (9). For greater accuracy, the viscometer can be calibrated with a fluid or fluids of known viscosities. The calibration parameter can be incorporated into Equation (9) by adding a coefficient to the right-hand side. The coefficient, which is possibly a function of the position of the float and flow rate of the fluid, would be determined experimentally. Therefore, Equation (9) would become:

$$\eta F(x) = \frac{C(x,Q) \pi R_f^4 (\rho_f - \rho) g_x}{8Q} \quad (10)$$

where $C(x,Q)$ is the added coefficient. If $C(x,Q)$ is first assumed independent of the flow rate, $C(x,Q)$ can be experimentally measured by varying the flow rate of the calibrating fluid of known viscosity and observing the changes in float height. If several fluids of known but different viscosities are used in the calibration and the flow regulated so as to position the float at the same height, the effects of the flow rate on the added coefficient might be determined. Once the value of the right-hand side of Equation (10) is known, the viscosity can be determined from the position of the float.

To illustrate the sensitivity of the viscosity to changes in the position of the float, sample calculations were made. The calibrating fluid had an assumed viscosity of 1 centipoise. The flow conditions of the assumed calibrating fluid were such that the right-hand side of Equation (10) had a value of 100 centipoise when the observed position of the float was 40 centimeters above the position where $x = 0$. The dimensions of the viscometer are those listed in Figure 1. Values of the viscosity were computed for 20-centimeter incremental changes in float height and flow conditions resulting in a value of 100 centipoise for the right-hand side of Equation (10).

RESULTS AND CONCLUSIONS

The equation relating the viscosity of a fluid to the position of the float for the proposed viscometer is:

$$\eta F(x) = \frac{C(x,Q) \pi R_f^4 (\rho_f - \rho) g_x}{8Q} \quad (10)$$

where

$$F(x) = \frac{k^2 \left[\frac{(1 - k^2)}{2 \ln(1/k)} \right]}{\left[(1 - k^4) - \frac{(1 - k^2)^2}{\ln(1/k)} \right]}$$

$$k = R_f / (R_f + x \tan \theta)$$

and

$C(x,Q)$ is an experimentally determined coefficient.

Equation (10) is limited to a steady, laminar, Newtonian flow of an incompressible fluid.

Solutions to Equation (10) were computed for a viscometer with dimensions given in Figure 1. Results of the calculations are given in Figure 3. These results indicate that the position of the float is almost proportional to the square root of the viscosity.

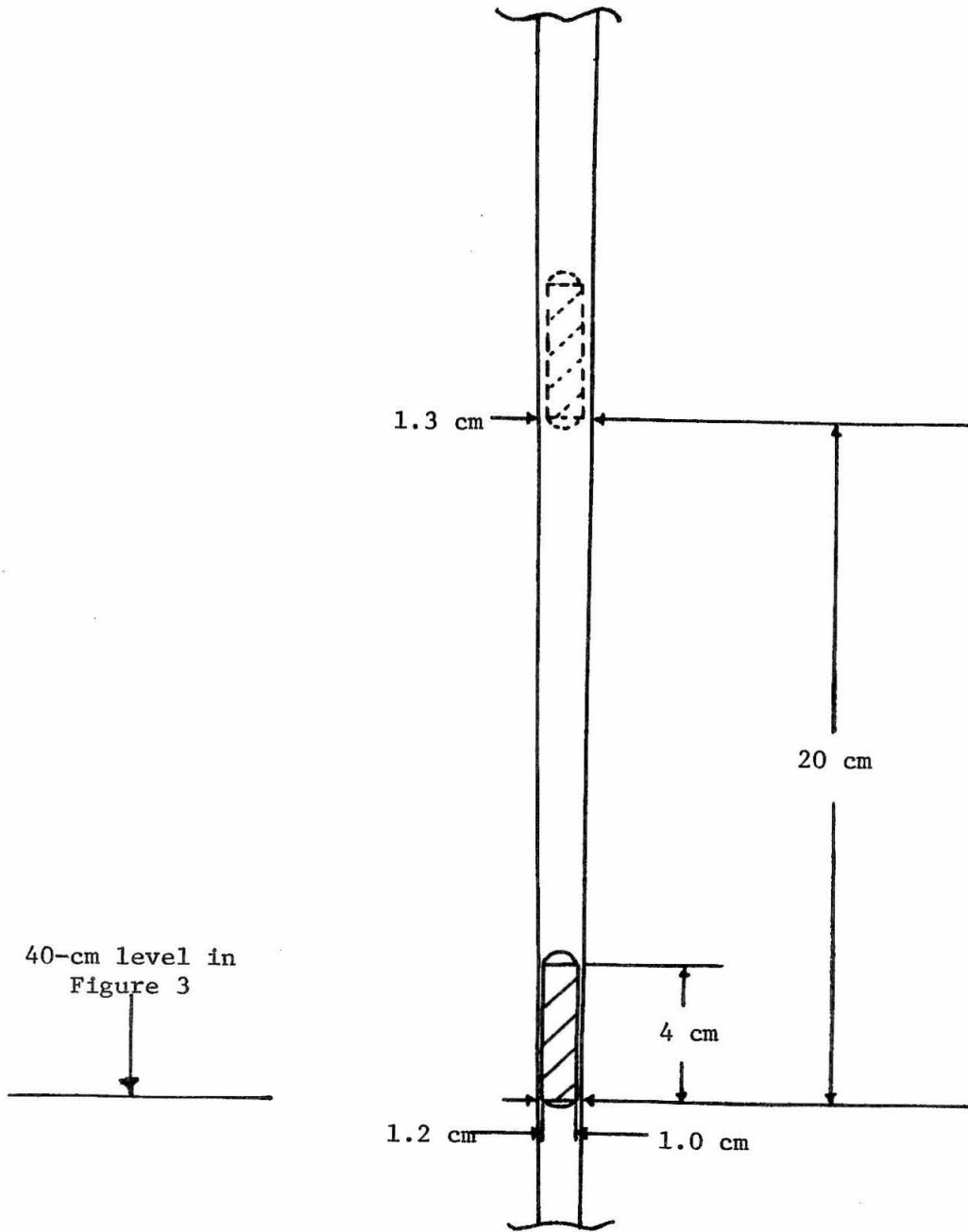


Fig. 1. Proposed Viscometer Design

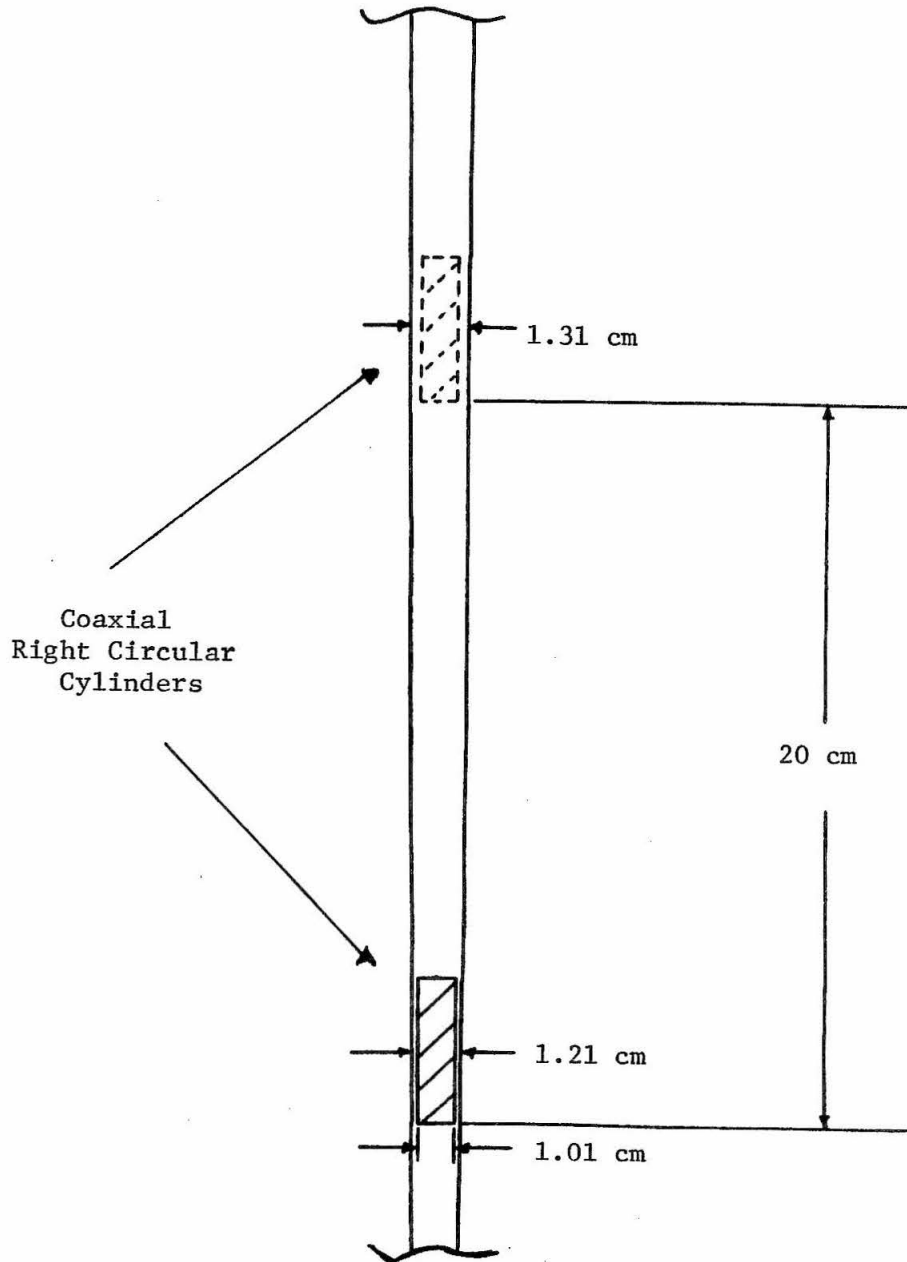


Fig. 2. Viscometer Design Assumed

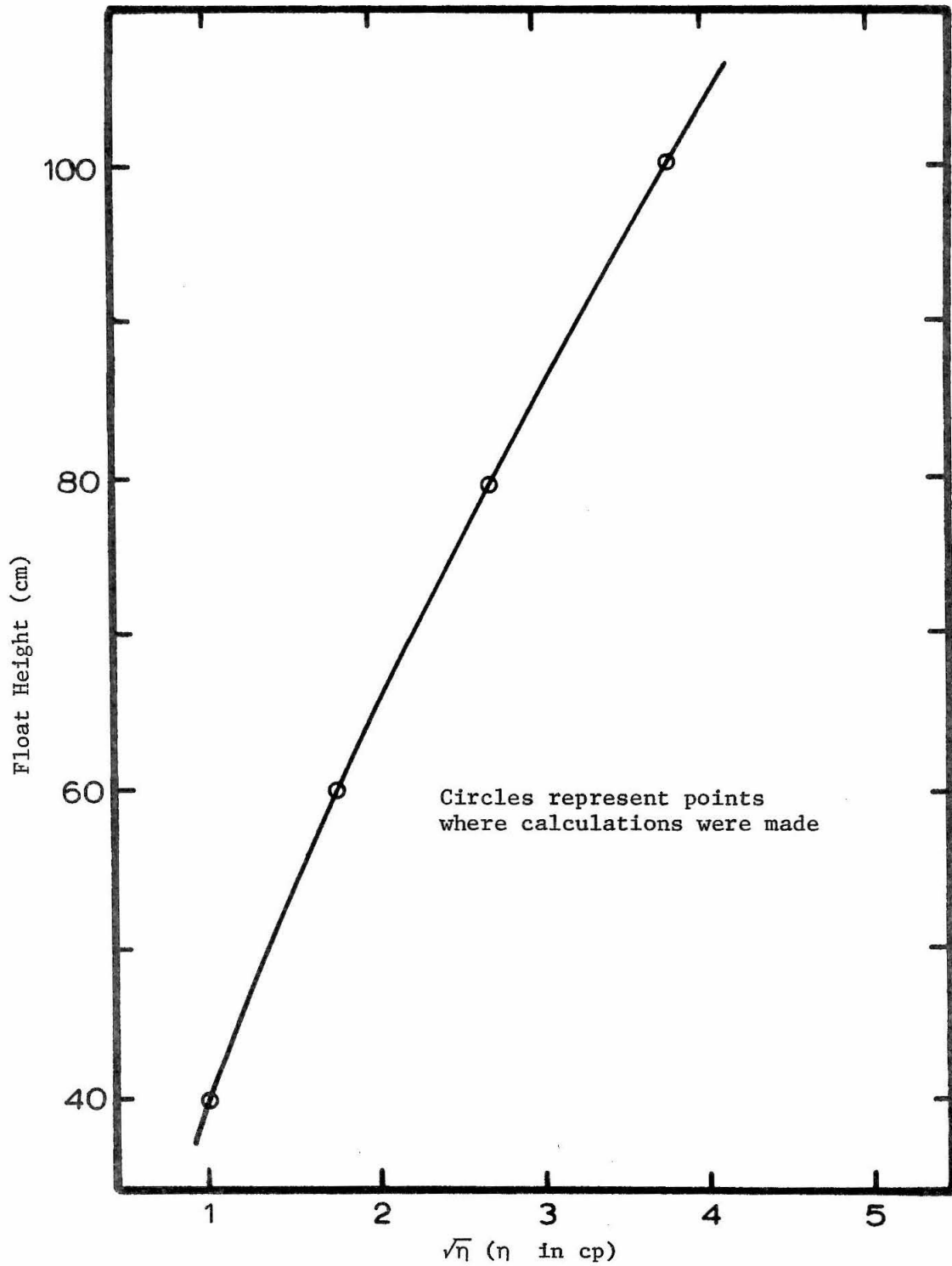


Fig. 3. Float Height vs Viscosity for Proposed Viscometer

REFERENCES

1. Foust, A. S., Wenzel, L. A., Clump, Maus L., and Anderson, B. L., Principles of Unit Operations, Wiley & Sons, New York (1960), pp. 409-411.
2. McCabe, W. J., and Smith, J. C., Unit Operations of Chemical Engineering, McGraw-Hill, New York (1956), pp. 117-123.
3. Schoenborn, E. M., and Colburn, A. P., Trans. Am. Inst. Chem. Engrs. 35, (1939) p. 359.
4. Bird, R. B., Stewart, W. E., and Lightfoot, E. N., Transport Phenomena, Wiley & Sons, New York (1960), pp. 51-54.

NOTATION

A	cross sectional area of float
A_s	surface area of side of float
$C(x,Q)$	experimental correction factor
g_x	gravitational force in x coordinate direction
k	relationship between radii of coaxial right-circular cylinders, $R_{inner} = kR_{outer}$
L_f	length of float
\ln	natural logarithm
P	Pressure
Q	volumetric flow rate
R	inside radius of outer coaxial cylinder
V_f	volume of float
V_x	average velocity in annular region
x	coordinate representing vertical direction
z	coordinate representing actual direction of flow in annular region
θ	angle between the x and y coordinate directions
η	viscosity of fluid
ρ	density of fluid
ρ_f	density of float

Subscripts

1	bottom of float
2	top of float
12	arithmetic mean of top and bottom of float
f	float
s	side